

Simulating financial time series using attention

Weilong Fu*, Ali Hirsas†, Jörg Osterrieder‡

Abstract

Financial time series simulation is a central topic since it extends the limited real data for training and evaluation of trading strategies. It is also challenging because of the complex statistical properties of the real financial data. We introduce two generative adversarial networks (GANs), which utilize the convolutional networks with attention and the transformers, for financial time series simulation. The GANs learn the statistical properties in a data-driven manner and the attention mechanism helps to replicate the long-range dependencies. The proposed GANs are tested on the S&P 500 index and option data, examined by scores based on the stylized facts and are compared with the pure convolutional GAN, i.e. **QuantGAN**. The attention-based GANs not only reproduce the stylized facts, but also smooth the autocorrelation of returns.

Keywords: deep learning, generative adversarial networks, attention, time series, stylized facts

1 Introduction

Training and evaluation of trading strategies need lots of data. Due to the limited amount of real data, there is a growing need to be able to simulate realistic financial data which satisfies the stylized facts. There has already been a vast literature of financial time series models. The generalized autoregressive conditional heteroskedasticity (GARCH) [5] model and its variants are applied to the stock prices and indices. The Black-Merton-Scholes model [4], the Heston model [19], the variance gamma model [30], etc. are applied to the option surfaces. The parametric models are popular for their simplicity, mathematical explicitness and robustness. However, it is difficult for a parametric model to fit all the major stylized facts.

Recently, more data-driven approaches based on generative adversarial networks (GANs) [16] are proposed to deal with the problem. The GAN includes a generator, which is used to generate samples, and a discriminator, which is responsible for judging whether the generated samples are similar enough to the real data. The applications of GANs to financial time series range from the underlying asset price prediction [44, 43, 27] and simulation [34, 13, 25, 15, 39] to the option surface simulation [38]. Some more GANs of time series are proposed in [35, 32, 14, 8, 41, 26] and some more generative models of time series are in [21, 33, 40]. However, the network structures of the GANs in financial time series simulation are mostly limited in convolutional networks [28] and recurrent networks [20, 10].

There have been various different GANs which employ the attention mechanism [3, 29] to improve their performance, e.g., the convolutional networks with attention [42, 6, 12], and the transformer networks [24, 22]. But the attention mechanism has not been tested on financial time series. It is shown in [39] that long-range dependency is a major challenge in financial time series simulation. The attention mechanism [3, 29] is perfectly suitable for modeling the stylized facts of long-range dependency due to the large receptive field size of the attention layer. Thus we are motivated to use the attention-based GANs to simulate the financial time series. It is important to note the

*Department of IEOR, Columbia University, wf2232@columbia.edu

†Department of IEOR, Columbia University, ah2347@columbia.edu

‡School of Engineering, Zurich University of Applied Sciences, oste@zhaw.ch

difference between time series and fixed-dimensional variables, since a time series can have an arbitrary length. Thus we need to modify the attention-based GANs to make it agnostic to the length of the time series by changing all the layers in the generator to the causal layers. Our findings based on numerical results show that the attention-based GANs perform as well as the temporal convolutional network (WaveNet [35]) in replication of the major stylized facts, including heavy tails, autocorrelation and cross-correlation, and are better at simulating smooth autocorrelation of returns and satisfying the no-arbitrage condition of option surfaces. It is well known in the literature that both GANs and transformers [36], which contain multiple attention layers, are hard to train, and it is a challenging problem to combine them together. Millions or billions of samples are usually used to train the transformer GANs in text generation and image simulation. Authors in [24] pointed it out that transformers are data-hungry, and thus they made use of data augmentation techniques to improve the transformer GANs. In this paper, we propose a new transformer GAN using sparse attention [9, 12] and train it using a small amount of financial time series data (around 3000 samples).

The rest of this paper is organized as follows. In Section 2, we define the generative model and emphasize the difference between the generative models of time series and fixed-dimensional distributions. We also introduce the GANs, which employ a discriminator to train the generator. In Section 3, we introduce and compare the regular and causal convolutional layers and attention layers, which are building blocks of the proposed GANs. In Section 4, we propose to employ attention as the tool to model the long-range dependencies, and give the detailed structure of the proposed temporal attention GAN (TAGAN) and temporal transformer GAN (TTGAN). In Sections 5 and 6, we show the numerical results of the proposed GANs for the S&P 500 index simulation and its index option surface simulation respectively. Most graphical results are collected in Appendix A. Section 7 summarizes the paper.

2 Generative model of financial time series

2.1 Problem formulation

Suppose we have a financial time series $\{\mathbf{x}_t \in \mathbb{R}^d\}_{t \in \mathbb{Z}}$, e.g., the historical of prices or volatilities, and would like to generate a time series $\{\mathbf{y}_t \in \mathbb{R}^d\}_{t \in \mathbb{Z}}$ that has the same statistical properties given a series of i.i.d. random noise $\{\mathbf{z}_t \in \mathbb{R}^{d_n}\}_{t \in \mathbb{Z}}$ via deep learning. Let $\mathbf{z}_{i:j}$ denote the sequence $\{\mathbf{z}_i, \mathbf{z}_{i+1}, \dots, \mathbf{z}_j\}$ and the same notation is used for all time series hereafter.

Here we follow the definition of the *neural process* in [39]. We would like to develop a generator $G(\cdot; \theta_G)$, a neural network with the parameter $\theta_G \in \Theta_G$, which takes random noise from $\{\mathbf{z}_t\}_{t \in \mathbb{Z}}$ as its input and outputs the time series $\{\mathbf{y}_t\}_{t \in \mathbb{Z}}$, i.e.,

$$\mathbf{y}_t = G(\mathbf{z}_{t-f+1:t}; \theta_G), \forall t \in \mathbb{Z}$$

where $f > 0$ is called the receptive field size (RFS) and means the length of noise variables of which \mathbf{y}_t is composed. By this definition, \mathbf{y}_t and $\mathbf{y}_{t+\tau}$ would be independent if $\tau \geq f$. Also, since \mathbf{y}_t is computed from $\{\mathbf{z}_\tau\}_{\tau \leq t}$, we know $\{\mathbf{y}_t\}_{t \in \mathbb{Z}}$ is adapted to $\{\mathbf{z}_t\}_{t \in \mathbb{Z}}$.

The generator of time series has to satisfy the following conditions that make it different from a generator of a fixed-dimensional distribution.

- (a) The generator should be able to take in random noise of length $l + f - 1$ to output the aimed time series of an arbitrary length l , i.e.,

$$\mathbf{y}_{t-l+1:t} = G(\mathbf{z}_{t-l-f+2:t}; \theta_G), \forall t \in \mathbb{Z}.$$

- (b) The generated time series can be prolonged in a consistent manner. For arbitrary $t_1, t_2, t_3, t_4 \in \mathbb{Z}$ such that $[t_1, t_2] \cap [t_3, t_4] \neq \emptyset$,

$$\mathbf{y}_{t_1:t_2} = G(\mathbf{z}_{t_1-f+1:t_2}; \theta_G)$$

and

$$\tilde{\mathbf{y}}_{t_3:t_4} = G(\mathbf{z}_{t_3-f+1:t_4}; \theta_G),$$

the overlapping part of the generated time series must be equal, i.e.,

$$\mathbf{y}_{\max\{t_1, t_3\}:\min\{t_2, t_4\}} = \tilde{\mathbf{y}}_{\max\{t_1, t_3\}:\min\{t_2, t_4\}}.$$

This means the generated time series $\{\mathbf{y}_t\}_{t \in \mathbb{Z}}$ is uniquely determined by the random noise series $\{\mathbf{z}_t\}_{t \in \mathbb{Z}}$.

Given the two conditions are satisfied, we can always let the generator $G(\cdot; \theta_G)$ compute sequences of length l and then combine the sequences to make up a longer sequence $\mathbf{y}_{1:T}$, where $T > l$. To be more specific, we first calculate the pieces

$$\mathbf{y}_{(i-1)l+1:i} = G(\mathbf{z}_{(i-1)l-f+2:i}; \theta_G), \forall 1 \leq i \leq \lceil T/l \rceil,$$

and then $\mathbf{y}_{1:T}$ is a subsequence of $\mathbf{y}_{1:l \lceil T/l \rceil}$, where $\lceil \cdot \rceil$ is the ceiling function.

2.2 Training through generative adversarial network

We give a quick introduction of generative adversarial networks (GANs) as well as the loss functions for training GANs. The GAN introduces a discriminator

$$D(\cdot; \theta_D) : \mathbb{R}^{l \times d} \rightarrow \mathbb{R},$$

where $\theta_D \in \Theta_D$, to evaluate the similarity between the real historical data $\{\mathbf{x}_t\}_{t \in \mathbb{Z}}$ and the simulated data $\{\mathbf{y}_t\}_{t \in \mathbb{Z}}$. A higher output value from $D(\cdot; \theta_D)$ means the discriminator holds a stronger belief that the input sample comes from the real data.

Suppose we have a sequence of real data $\mathbf{x}_{1:T}$. Let $\mathbb{P}_{\mathbf{X}}$ be the uniform distribution over the window data of length l , $\{\mathbf{x}_{i:i+l-1}, \forall 1 \leq i \leq T-l+1\}$. Also, let $\mathbb{P}_{\mathbf{Z}}$ be distribution of $\mathbf{z}_{1:l+f-1}$. Then we draw $\mathbf{X} \sim \mathbb{P}_{\mathbf{X}}$ to be a piece of real data of length l and $\mathbf{Z} \sim \mathbb{P}_{\mathbf{Z}}$ the random noise of length $l+f-1$ and get the simulated sequence $\mathbf{Y} = G(\mathbf{Z}; \theta_G) \in \mathbb{R}^{l \times d}$. The GAN trains the generator and the discriminator by minimizing the following loss functions

$$\min_{\theta_G} \mathbb{E}_{\mathbf{Z}} \mathcal{L}_G(D(G(\mathbf{Z}; \theta_G); \theta_D))$$

and

$$\min_{\theta_D} \mathbb{E}_{\mathbf{X}, \mathbf{Z}, \tilde{\mathbf{X}}} \mathcal{L}_D(D(\mathbf{X}; \theta_D), D(G(\mathbf{Z}; \theta_G); \theta_D), \nabla_{\tilde{\mathbf{X}}} D(\tilde{\mathbf{X}}; \theta_D)),$$

where $\mathcal{L}_G(\cdot)$ and $\mathcal{L}_D(\cdot, \cdot, \cdot)$ are the loss functions of the discriminator and the generator. The third argument in $\mathcal{L}_D(\cdot, \cdot, \cdot)$ is not included in the original GAN but related with gradient penalty, where $\tilde{\mathbf{X}} = (1-U)\mathbf{X} + U\mathbf{Y}$ is a linear interpolation between \mathbf{X} and \mathbf{Y} requiring U follows the uniform distribution over $(0, 1)$.

The loss functions of the original GAN [16] are

$$\begin{aligned} \mathcal{L}_G(d_f) &= -\ln(\sigma(d_f)) \\ \mathcal{L}_D(d_r, d_f, \mathbf{g}) &= -\ln(\sigma(d_r)) - \ln(1 - \sigma(d_f)) \end{aligned} \quad (1)$$

where $\sigma(d) = 1/(1 + e^{-d})$ is the sigmoid function and $\sigma(D(\mathbf{X}; \theta_D))$ means the probability that the discriminator considers \mathbf{X} belongs to the real data. A quick derivation of the losses is included in Appendix C.

Besides the original losses, the loss functions of the Wasserstein GAN [1] with gradient penalty (WGAN-GP) [17] are also widely used, where the gradient norm penalty is used to achieve Lipschitz continuity:

$$\begin{aligned} \mathcal{L}_G(d_f) &= -d_f \\ \mathcal{L}_D(d_r, d_f, \mathbf{g}) &= -d_r + d_f + \lambda(\|\mathbf{g}\| - 1)^2 \end{aligned} \quad (2)$$

where λ is a constant and $\lambda = 10$ by default. $\|\cdot\|$ is the Frobenius norm. In Appendix C, we introduce how the losses are derived.

3 Network layers

In this section, we going to list all the layers that will be used in the proposed network structure. Some of the layers are already introduced in literature, but we still give a short introduction for each to make the paper self-contained. The layers are classified into regular layers and causal layers. In the causal layers, each output node only depends on the input nodes with equal or smaller time indices. Suppose the input of the causal layer is $\mathbf{I} \in \mathbb{R}^{n_l \times n_i}$ with rows $\{\mathbf{I}_{t,\cdot}\}_{t=1}^{n_l}$ and the output is $\mathbf{O} \in \mathbb{R}^{(n_l-f+1) \times n_o}$ with rows $\{\mathbf{O}_{t,\cdot}\}_{t=f}^{n_l}$, then each row of the output $\mathbf{O}_{t,\cdot}$ only depends on $\{\mathbf{I}_{\tau,\cdot}\}_{\tau=t-f+1}^t$. However, the regular layers are not subject to this restriction. Since the output of the generator needs to be adapted to the input noise, the causal layers are used in the generator. While the regular layers admit more flexibility and are used in the discriminator.

3.1 Regular convolutional layer

In [28], the authors proposed the convolutional layer, which is good at extracting local information. The two-dimensional case is widely used in computer vision and the one-dimensional case is used in sequence models. Although the convolutional layer is widely used and well-known, we reiterate the definition to show the difference between the different layers. Suppose the input is $\mathbf{I} \in \mathbb{R}^{n_l \times n_i}$ and it passes through a one-dimensional regular convolutional layer with kernel size n_k , output channel n_o and stride s . The kernel size n_k is an odd number by default. The parameters are the weight $\mathbf{W} \in \mathbb{R}^{n_k \times n_i \times n_o}$ and the intercept $\mathbf{b} \in \mathbb{R}^{n_o}$. The output of the regular convolutional layer is $\mathbf{O} \in \mathbb{R}^{\lfloor n_l/s \rfloor \times n_o}$ given by

$$O_{i_l, i_o} = \sum_{i=1}^{n_i} \sum_{i_k=1}^{n_k} W_{i_k, i, i_o} I_{s(i_l-1)+1-(n_k+1)/2+i_k, i} + b_{i_o}, \forall 1 \leq i_l \leq \lfloor n_l/s \rfloor, 1 \leq i_o \leq n_o,$$

where $\lfloor \cdot \rfloor$ is the floor function. The ‘same’ padding rule is applied to the input, i.e., $I_{i_l, i} = I_{1, i}, \forall i_l < 1$ and $I_{i_l, i} = I_{n_l, i}, \forall i_l > n_l$. The regular convolutional layer is illustrated in Figure 1. It is denoted as $\text{conv}_{\tau}^{(n_k, n_o, s)}(\cdot)$, where n_k, n_o and s are the kernel size, output channel and stride respectively.

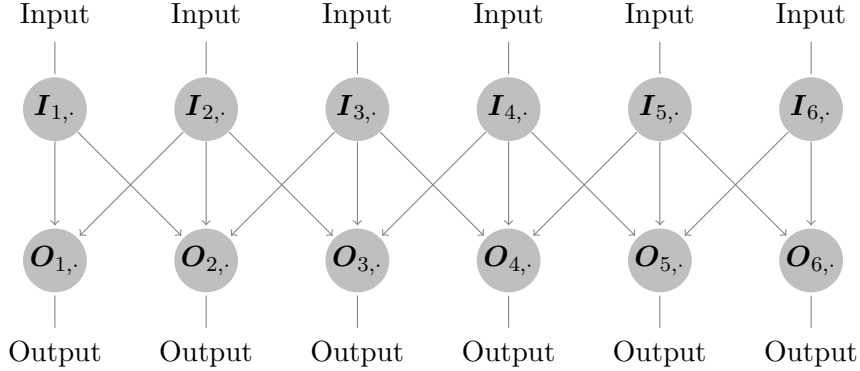


Figure 1: Illustration of the regular convolutional layer (length $n_l = 6$, kernel size $n_k = 3$ and stride $s = 1$).

3.2 Causal convolutional layer

In [35], the authors proposed the causal convolutional layer to model the audio data. Suppose the input is $\mathbf{I} \in \mathbb{R}^{n_l \times n_i}$ and it passes through a causal convolutional layer with kernel size n_k and output channel n_o . The parameters are the weight $\mathbf{W} \in \mathbb{R}^{n_k \times n_i \times n_o}$ and the intercept $\mathbf{b} \in \mathbb{R}^{n_o}$. The output of the causal convolutional layer

is $\mathbf{O} \in \mathbb{R}^{(n_l - n_k + 1) \times n_o}$. In the causal layer, the time index of the output is taken from $\{n_k, n_k + 1, \dots, n_l\}$. The output is given by

$$O_{t, i_o} = \sum_{i=1}^{n_i} \sum_{i_k=1}^{n_k} W_{i_k, i, i_o} I_{t-n_k+i_k, i} + b_{i_o}, \forall n_k \leq t \leq n_l, 1 \leq i_o \leq n_o.$$

The RFS of the causal convolutional layer is equal to n_k . The causal convolutional layer is illustrated in Figure 2. It is denoted as $\text{conv}_c^{(n_k, n_o)}(\cdot)$, where n_k and n_o are the kernel size and output channel.

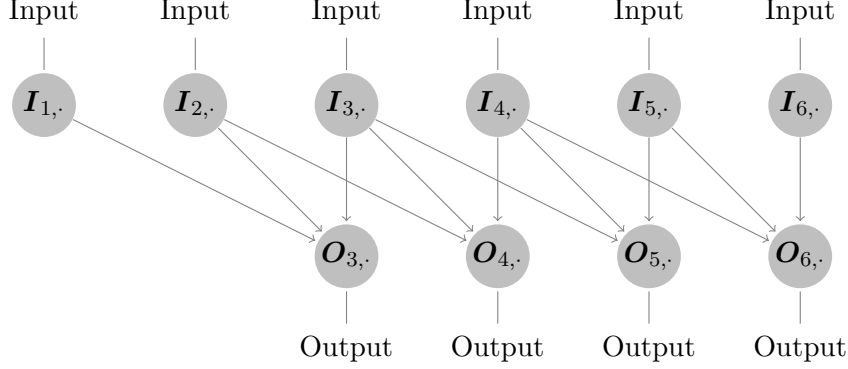


Figure 2: Illustration of the causal convolutional layer (length $n_l = 6$ and kernel size $n_k = 3$).

3.3 Regular attention layer

The attention layer was introduced by [3, 29]. It is designed to receive and process global information to improve the performance of convolutional or recurrent networks. The attention layer was first used in text translation, where input words and output words may follow different orders because of different grammar. So, the attention layer needs to search from the entire inputs to decide which input word is corresponding to a specific output word. The best match in the input becomes the ‘attention’ of the layer. Authors in [36] proposed the transformer network, which consists of only attention layers and multi-layer perceptrons, and proved attention layers are capable of modeling sequences without help from convolutional or recurrent layers. Suppose the input of the regular multi-head attention layer is $\mathbf{I} \in \mathbb{R}^{n_i \times n_i}$, the hidden size is n_a and the number of heads is n_h , which satisfy $\text{mod}(n_a, n_h) = 0$. The parameters are the weights $\mathbf{W}^Q, \mathbf{W}^K, \mathbf{W}^V \in \mathbb{R}^{n_i \times n_a}$, $\mathbf{W}^O \in \mathbb{R}^{n_a \times n_i}$ and intercepts $\mathbf{b}^Q, \mathbf{b}^K, \mathbf{b}^V \in \mathbb{R}^{n_a}$, $\mathbf{b}^O \in \mathbb{R}^{n_i}$. Let $\mathbf{1}$ be the vector of length n_i with all elements of 1. The formulae in the regular attention layer are

$$\begin{aligned} \mathbf{Q} &= \mathbf{I}\mathbf{W}^Q + \mathbf{1}\mathbf{b}^{Q\top} \\ \mathbf{K} &= \mathbf{I}\mathbf{W}^K + \mathbf{1}\mathbf{b}^{K\top} \\ \mathbf{V} &= \mathbf{I}\mathbf{W}^V + \mathbf{1}\mathbf{b}^{V\top} \\ \mathbf{A}_{(i_h)} &= \text{softmax} \left(\mathbf{Q}_{(i_h)} \mathbf{K}_{(i_h)}^\top \right) \mathbf{V}_{(i_h)}, \forall 1 \leq i_h \leq n_h \\ \mathbf{O} &= \mathbf{A}\mathbf{W}^O + \mathbf{1}\mathbf{b}^{O\top} \end{aligned} \quad (3)$$

where $\mathbf{A}_{(i_h)}$ means the submatrix from column $(i_h - 1)n_h + 1$ to column $i_h n_h$ and $\mathbf{O} \in \mathbb{R}^{n_i \times n_i}$ is the output of the attention layer. The softmax function is evaluated along each row of the input matrix. While the fourth equation in Equation (3) is often replaced with

$$\mathbf{A}_{(i_h)} = \text{softmax} \left(\mathbf{Q}_{(i_h)} \mathbf{K}_{(i_h)}^\top / \sqrt{n_a/n_h} \right) \mathbf{V}_{(i_h)}$$

when the size of a single attention head n_a/n_h is large, we stick with the equation in Equation (3) since it shows better empirical results when n_a/n_h is small. The dependence relationship of the output on the input in the regular attention layer is illustrated in Figure 3. The regular attention layer is denoted as $\text{attn}_r^{(n_a, n_h)}(\cdot)$, where n_a and n_h are the hidden size and number of heads.

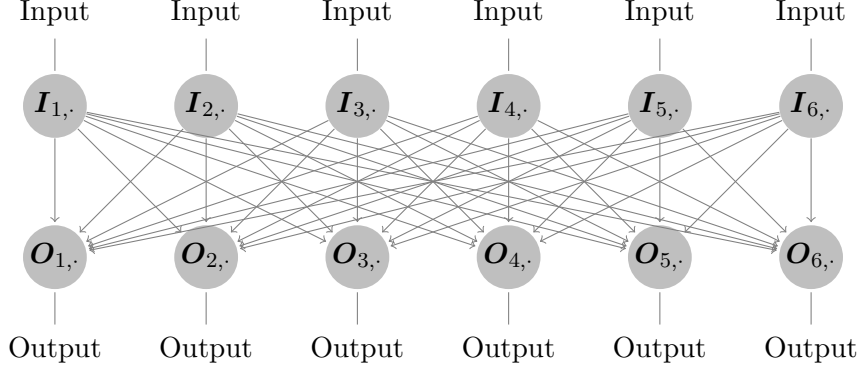


Figure 3: Dependence relationship in the regular attention layer (length $n_l = 6$).

3.4 Sparse attention layer

The sparse attention layer is introduced by [9] to accelerate computation and improve the focus of the attention layer. The sparse attention introduces the sparse masks before the softmax function, i.e. replacing the fourth equation in Equation (3) with

$$\mathbf{A}_{(i_h)} = \text{softmax} \left(\mathbf{Q}_{(i_h)} \mathbf{K}_{(i_h)}^\top + \mathbf{M}^{(i_h)} \right) \mathbf{V}_{(i_h)} \quad (4)$$

where $\mathbf{M}^{(i_h)} \in \mathbb{R}^{n_i \times n_i}, \forall 1 \leq i_h \leq n_h$ are the sparse mask matrices. In the mask $\mathbf{M}^{(i_h)}$, the elements in the masked positions are assigned a large negative value $-L$, while the elements outside the mask are assigned 0. Since they are sparse masks, the 0 elements are sparse and the large negative value elements are dense. The masked positions are mapped to 0 by the softmax function since $e^{-L} \approx 0$, where we usually let $L = 10^3$. In this way, the masked positions in $\mathbf{Q}_{(i_h)} \mathbf{K}_{(i_h)}^\top$ are not involved in the result of the softmax function and the attention is limited within the sparse mask.

In this paper we use the sparse masks proposed in [12]. They are generated in the following way. Let $s = \lfloor \sqrt{n_l} \rfloor$ be the stride, where $\lfloor \cdot \rfloor$ is the floor function. We then create the index sets for the masks:

- Left floor mask: $S_1 = \{(i, j) : \lfloor (i-1)/s \rfloor = \lfloor (j-1)/s \rfloor \text{ and } i \geq j\}$
- Right floor mask: $S_2 = \{(i, j) : \lfloor (i-1)/s \rfloor = \lfloor (j-1)/s \rfloor \text{ and } i \leq j\}$
- Left repetitive mask: $S_3 = \{(i, j) : \text{mod}(j, s) = 0 \text{ or } i = j\}$
- Right repetitive mask: $S_4 = \{(i, j) : \text{mod}(j, s) = 1 \text{ or } i = j\}$

The corresponding masks are defined as

$$M_{i,j}^{(i_h)} = \begin{cases} 0, & \text{if } (i, j) \in S_{i_s}, \\ -L, & \text{if } (i, j) \notin S_{i_s}, \end{cases} \text{ when } i_h \equiv i_s \pmod{4}.$$

As a result, the number of heads n_h needs to be a multiple of 4 when we use the sparse attention. The sparse attention limits the attention of each node to a specific region such that the network would converge faster. In Figure 4, we show an example of the sparse masks. As shown in Figure 4, the left and right floor masks focus on local features and the left and right repetitive masks focus on periodic features. The sparse attention layer is denoted as $\text{attn}_s^{(n_a, n_h)}(\cdot)$, where n_a and n_h are the hidden size and number of heads.

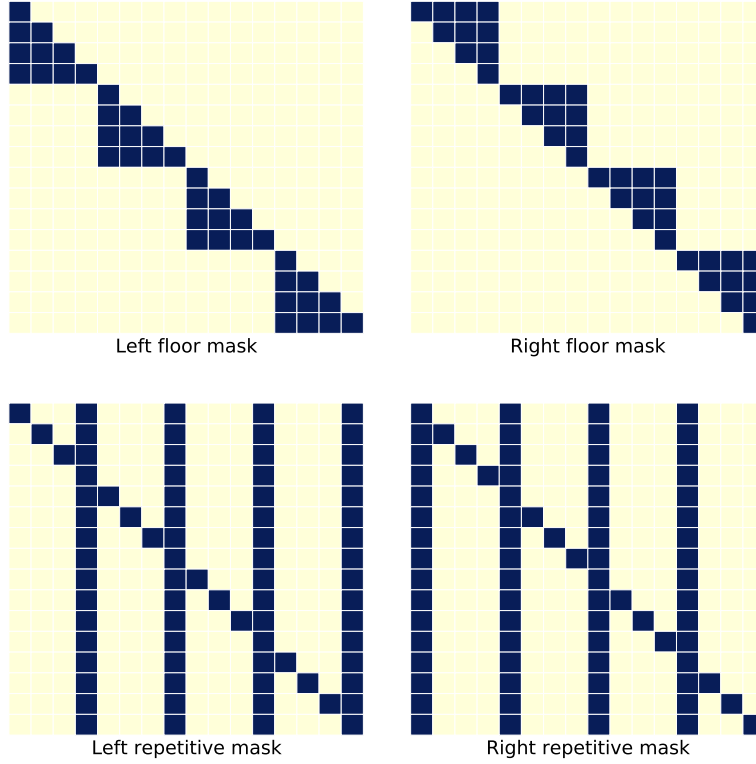


Figure 4: Example of the sparse masks when $n_l = 16$. Light elements are masked while dark elements are not.

3.5 Causal attention layer

To make use of the attention layers in the generator of time series, we need to make sure the output only depends on the input elements in the past. This is also achieved by using masks. We suppose the same input $\mathbf{I} \in \mathbb{R}^{n_l \times n_i}$ as before, and the parameters are defined the same as in the regular attention. Let the RFS of the layer be n_f . The definition of the attention layer in Equation (3) needs to be replaced with

$$\begin{aligned}
 \mathbf{Q} &= \mathbf{I}\mathbf{W}^Q + \mathbf{1}\mathbf{b}^{Q\top} \\
 \mathbf{K} &= \mathbf{I}\mathbf{W}^K + \mathbf{1}\mathbf{b}^{K\top} \\
 \mathbf{V} &= \mathbf{I}\mathbf{W}^V + \mathbf{1}\mathbf{b}^{V\top} \\
 \mathbf{A}_{(i_h)} &= \text{softmax} \left(\mathbf{Q}_{(i_h)} \mathbf{K}_{(i_h)}^\top + \mathbf{M} \right) \mathbf{V}_{(i_h)}, \forall 1 \leq i_h \leq n_h \\
 \mathbf{O} &= \left(\mathbf{A}\mathbf{W}^O + \mathbf{1}\mathbf{b}^{O\top} \right)_{n_f:n_l, \cdot}
 \end{aligned}$$

where $(\cdot)_{n_f:n_l, \cdot}$ means the submatrix from row n_f to row n_l , and \mathbf{M} is a mask matrix with the elements

$$M_{i,j} = \begin{cases} 0, & \text{if } 0 \leq i - j \leq n_f - 1, \\ -L, & \text{else.} \end{cases}$$

In this way, each output only depends on the current input and $n_f - 1$ past inputs. The benefit of the causal attention layer is that it can increase the RFS n_f arbitrarily without introducing additional parameters. The size of the parameters does not depend on the input length n_l or the RFS n_f . The dependence relationship of the output on the input in the causal attention layer is illustrated in Figure 5. The causal

attention layer is denoted as $\text{attn}_c^{(n_a, n_h, n_f)}(\cdot)$, where n_a , n_h and n_f are the hidden size, number of heads and RFS respectively.

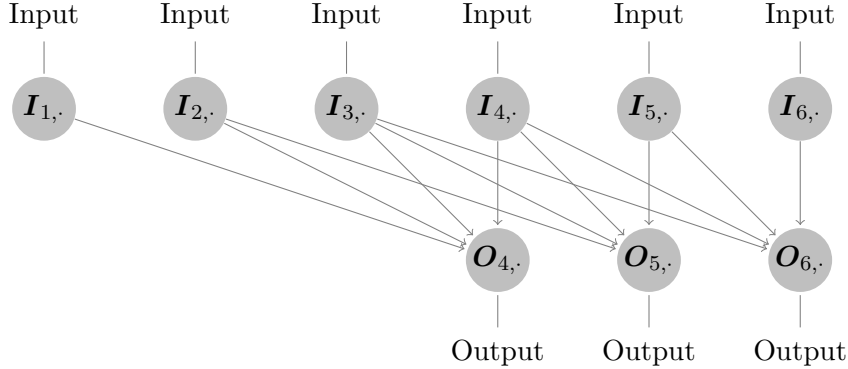


Figure 5: Dependence relationship in the causal attention layer (length $n_l = 6$ and RFS $n_f = 4$).

3.6 Multi-layer perceptron block

The multi-layer perceptron (MLP) is a key component of the transformer architecture. Suppose the input is $\mathbf{I} \in \mathbb{R}^{n_i \times n_i}$, the hidden size is n_m and the activation function is $h(\cdot)$. The parameters are the weights $\mathbf{W}^{(1)} \in \mathbb{R}^{n_i \times n_m}$, $\mathbf{W}^{(2)} \in \mathbb{R}^{n_m \times n_i}$ and intercepts $\mathbf{b}^{(1)} \in \mathbb{R}^{n_m}$, $\mathbf{b}^{(2)} \in \mathbb{R}^{n_i}$. Let $\mathbf{1}$ be the vector of length n_l with all elements of 1. The formulae in the MLP block are

$$\begin{aligned} \mathbf{H} &= \mathbf{I}\mathbf{W}^{(1)} + \mathbf{1}\mathbf{b}^{(1)\top} \\ \mathbf{O} &= h(\mathbf{H})\mathbf{W}^{(2)} + \mathbf{1}\mathbf{b}^{(2)\top} \end{aligned}$$

where the activation function $h(\cdot)$ is applied element-wise and $\mathbf{O} \in \mathbb{R}^{n_l \times n_i}$ is the output. All the activation functions will be applied element-wise in the paper. The MLP block is denoted as $\text{mlp}^{(n_m, h)}(\cdot)$, where n_m and $h(\cdot)$ are the hidden size and the activation function respectively.

4 Network structures

4.1 Need for a large receptive field size

The difficulty of financial time series simulation is to model the long-range dependencies. Figure 6 shows the autocorrelation of absolute values of the returns of the S&P 500 index from May 2010 to November 2018. The autocorrelation is positive, inferring the asset returns admit phases of high activity and low activity in terms of price changes. This stylized fact is called volatility clustering. The positive correlation decays to almost 0 when the lag is greater than 100. This means we need a generator of RFS larger than 100 to model the positive correlation in this data. Authors in [35, 39] make use of the temporal convolutional network (TCN) to increase the RFS. While in this paper we use the attention layer to build a generator of a large RFS.

4.2 Temporal attention GAN

The temporal attention GAN (TAGAN) is composed of a generator and a discriminator which are both convolutional networks with one self-attention layer. In the generator, we always use the causal layers while in the discriminator we only use the regular layers. This proposed model is the modification to the self-attention GAN [42] which has shown good performance in image generation. The hyper-parameters of TAGAN are listed in Table 1.

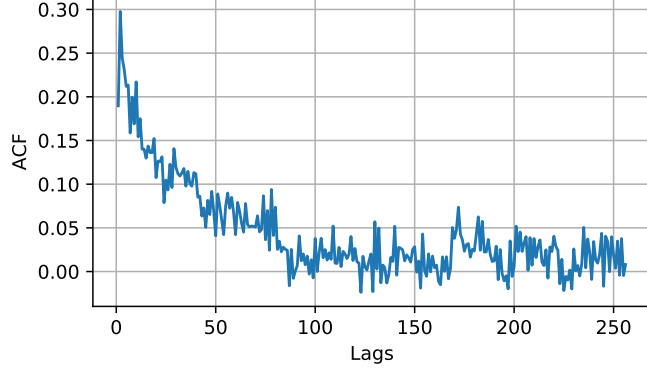


Figure 6: ACF of absolute values of the S&P 500 index returns.

hyper-parameter	meaning
l	data length
f	receptive field size
d_n	noise channel
d	data channel
d_h	hidden channel in the generator
d_s	start hidden channel in the discriminator
d_m	max hidden channel in the discriminator
n_k	kernel size in convolutions
L_1^G/L_2^G	number of convolutional blocks before/after attention in the generator
L_1^D/L_2^D	number of convolutional blocks before/after attention in the discriminator
n_h	number of heads in attention
$n_{a,G}/n_{a,D}$	attention hidden size in the generator/discriminator
$h_G(\cdot)/h_D(\cdot)$	activation function in the generator/discriminator

Table 1: Hyper-parameters in TAGAN.

Suppose the input noise of the generator is $\mathbf{Z} \in \mathbb{R}^{(l+f-1) \times d_n}$ and the output sample is $\mathbf{Y} \in \mathbb{R}^{l \times d}$. With the notations of the network layers introduced in Section 3, the generator can be written as follows

$$\begin{aligned}
\mathbf{H}^{(0)} &= \text{conv}_c^{(1,d_h)}(\mathbf{Z}) \\
\mathbf{H}^{(j)} &= \text{conv}_c^{(n_k,d_h)} \circ h_G \circ \text{conv}_c^{(n_k,d_h)} \circ h_G(\mathbf{H}^{(j-1)}), \forall 1 \leq j \leq L_1^G \\
\mathbf{H}^{(L_1^G+1)} &= \text{attn}_c^{(n_{a,G},n_h,f-2(L_1+L_2)(n_k-1))}(\mathbf{H}^{(L_1^G)}) \\
\mathbf{H}^{(j)} &= \text{conv}_c^{(n_k,d_h)} \circ h_G \circ \text{conv}_c^{(n_k,d_h)} \circ h_G(\mathbf{H}^{(j-1)}), \forall L_1^G + 2 \leq j \leq L_2^G + 1 \\
\mathbf{Y} &= \text{conv}_c^{(1,d)} \circ h_G(\mathbf{H}^{(L_2^G+1)})
\end{aligned}$$

where \circ means composition of the layers. The attention layer is embedded in the middle of the network to extend the receptive field and the convolutional layers are responsible for learning the local characteristics. The network structure of the generator of TAGAN is illustrated in Figure 7.

Let $\mathbf{Y} \in \mathbb{R}^{l \times d}$ denote either the real data or the fake data from the generator and $D(\mathbf{Y}; \theta_D)$ be the output of the discriminator. For the notation simplicity, we let

$$\begin{aligned}
\zeta_1^{(j)} &= \text{conv}_r^{(n_k, \min(2^{j-1}d_s, d_m), 1)} \\
\zeta_2^{(j)} &= \text{conv}_r^{(n_k, \min(2^{j-1}d_s, d_m), 2)}.
\end{aligned}$$

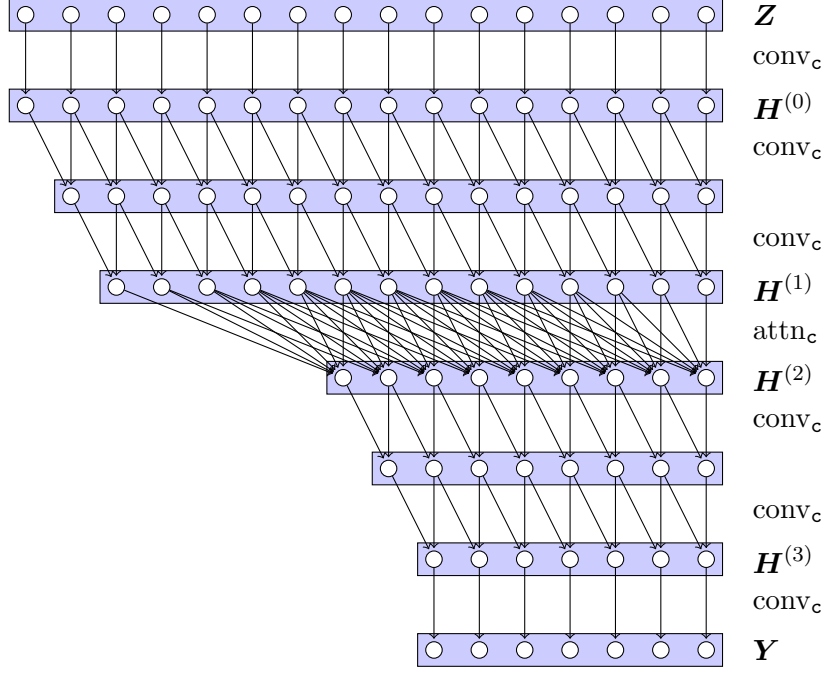


Figure 7: Illustration of the generator of TAGAN with $n_k = 2$ and $L_2^G = L_2^G = 1$.

Then the discriminator can be written as follows:

$$\begin{aligned}
\mathbf{U}^{(0)} &= \mathbf{Y} \\
\mathbf{U}^{(j)} &= \zeta_2^{(j)} \circ h_D \circ \zeta_1^{(j)} \circ h_D \left(\mathbf{U}^{(j-1)} \right), \forall 1 \leq j \leq L_1^D \\
\mathbf{U}^{(L_1^D+1)} &= \text{attn}_{\mathbf{r}}^{(n_a, D, n_h)} \left(\mathbf{U}^{(L_1^D)} \right) \\
\mathbf{U}^{(j)} &= \zeta_2^{(j-1)} \circ h_D \circ \zeta_1^{(j-1)} \circ h_D \left(\mathbf{U}^{(j-1)} \right), \forall L_1^D + 2 \leq j \leq L_2^D + 1 \\
D(\mathbf{Y}; \theta_D) &= \sum_{i_1=1}^{n_l} \sum_{i_2=1}^{\min(2^{L_1^D+L_2^D-1} d_s, d_m)} h_D \left(U_{i_1, i_2}^{(L_2^D+1)} \right) w_{i_2}
\end{aligned}$$

where $\mathbf{w} \in \mathbb{R}^{\min(2^{L_1^D+L_2^D-1} d_s, d_m)}$ is a trainable weight used before the output in the discriminator. The discriminator is the classical architecture of the convolutional network which shrinks the length but increases the channel of hidden layers.

We apply batch normalization [23] before activation functions, spectrum normalization [31] to the layer weights, and residual connections [18] and skip connections [39] to the generator and discriminator in TAGAN during training to stabilize the statistics of generated samples and improve the performance. Batch normalization normalizes the output of the layers, and the spectrum normalization limits the spectral norm of the weight parameters, both of which reduce extreme values in the network. Residual connections and skip connections accelerate training when the networks become deep.

4.3 Temporal transformer GAN

The temporal transformer GAN (TTGAN) is composed of two transformer networks as its generator and discriminator. Similar models can be found in [24, 22]. A transformer consists of several attention layers with each layer followed by a two-layer MLP. We use the causal attention layers in the generator and the sparse attention layer in the discriminator. Each causal attention layer has a flexible RFS. The hyper-parameters of TTGAN are listed in Table 2.

Suppose the input noise of the generator is $\mathbf{Z} \in \mathbb{R}^{(l+f-1) \times d_n}$ and the output sample is $\mathbf{Y} \in \mathbb{R}^{l \times d}$. With the notations of the network layers introduced in Section 3, the

hyper-parameter	meaning
l	data length
f	receptive field size
d_n	noise channel
d	data channel
d_h	hidden channel
n_h	number of heads in attention
n_a	attention hidden size
L	number of attention layers
$\{f_j\}_{j=1}^L$	the RFS of attentions in the generator
n_m	hidden size in the multi-layer perceptron
$h(\cdot)$	activation function

Table 2: Hyper-parameters in TTGAN.

generator can be written as follows

$$\begin{aligned}
\mathbf{H}^{(0)} &= \text{conv}_c^{(1,d_h)}(\mathbf{Z}) \\
\mathbf{H}^{(j)} &= \text{mlp}^{(n_m,h)} \circ \text{attn}_c^{(n_a,n_h,f_j)}(\mathbf{H}^{(j-1)}), \forall 1 \leq j \leq L \\
\mathbf{Y} &= \text{conv}_c^{(1,d)}(\mathbf{H}^{(L)})
\end{aligned}$$

where \circ means composition of the layers. The RFS of each attention layer needs to satisfy the equation $f - 1 = \sum_{j=1}^L (f_j - 1)$. This is because the length shrinkage of each attention layer is equal to RFS-1 and the total length shrinkage is equal to the sum of the shrinkage of all attention layers. The network structure of the generator of TTGAN is illustrated in Figure 8. At a first glance at Figures 7 and 8, it seems as if there is no difference between attention layers and convolutional layers. However, one should note that the formula of attention layers is different from that of convolutional layers and the RFS of attention layers can be much larger.

Let $\mathbf{Y} \in \mathbb{R}^{l \times d}$ denote either the real data or the fake data from the generator and $D(\mathbf{Y}; \theta_D)$ be the output of the discriminator. The discriminator can be written as follows.

$$\begin{aligned}
\mathbf{U}^{(0)} &= \text{conv}_r^{(1,d_h,1)}(\mathbf{Y}) \\
\mathbf{U}^{(j)} &= \text{mlp}^{(n_m,h)} \circ \text{attn}_s^{(n_a,n_h)}(\mathbf{U}^{(j-1)}), \forall 1 \leq j \leq L \\
D(\mathbf{Y}; \theta_D) &= \sum_{i_1=1}^l \sum_{i_2=1}^{n_h} U_{i_1,i_2}^{(L)} W_{i_1,i_2}
\end{aligned}$$

where $\mathbf{W} \in \mathbb{R}^{l \times n_h}$ is a trainable weight used before the output in the discriminator. The discriminator is the classical architecture of the transformer encoder but with sparse attention.

We apply batch normalization [23] before each attention layer and MLP block, spectrum normalization [31] to the layer weights, residual connections [18] and skip connections [39] to the generator and discriminator in TTGAN during training to stabilize the statistics of generated samples and improve the performance.

5 Simulation of the S&P 500 index

In this section, we show the numerical results of the proposed networks for the S&P 500 index simulation.

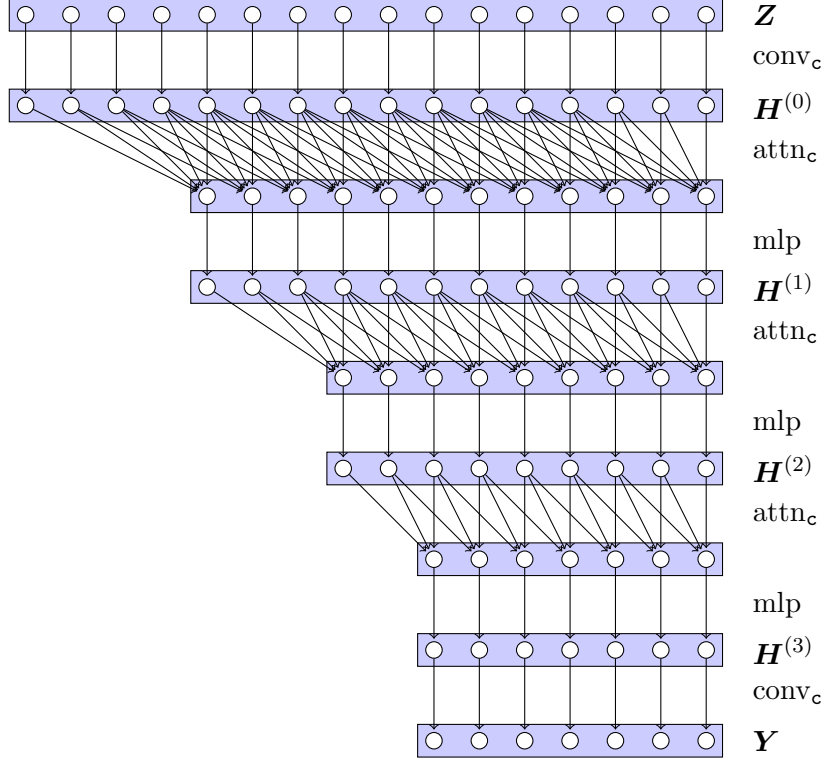


Figure 8: Illustration of the generator of TTGAN with $L = 3$ and $(f_1, f_2, f_3) = (5, 4, 3)$.

5.1 Stylized facts and metrics

It has been summarized in [11] that the returns of the S&P 500 index and also the equities admit the following characteristics called *stylized facts*:

- Asset returns shows heavier tails than the normal distribution.
- Escalator up and elevator down: large drawdowns but not equally large upward movements are observed.
- Autocorrelations of (daily) asset returns are often insignificant.
- Volatility clustering: volatility displays a positive autocorrelation.
- The autocorrelation function (ACF) of absolute returns decays slowly as a function of the time lag.
- Leverage effect: volatility of an asset is negatively correlated with the returns of that asset.

Suppose we have a sequence of historical prices $p_{0:T_x} = \{p_t\}_{t=0}^{T_x}$. We take the log returns to be the real data, i.e. $x_{1:T_x} = \{x_t\}_{t=1}^{T_x}$ where $x_t = \ln(p_t/p_{t-1})$. Then we sample N sequences of returns from the GAN and denote them as $\{y_{1:T}^{(i)}\}_{i=1}^N$. The evaluation metrics are listed as follows:

- The Wasserstein-1 distance of daily and multi-day returns. Let $F_\tau^h(x)$ denote the empirical CDF of the historical τ -day returns

$$\left\{ \sum_{j=0}^{\tau-1} x_{t+j} : 1 \leq t \leq T_x - \tau + 1 \right\}$$

and $F_\tau^g(x)$ the empirical CDF of the generated τ -day returns

$$\left\{ \sum_{j=0}^{\tau-1} y_{t+j}^{(i)} : 1 \leq i \leq N, 1 \leq t \leq T_x - \tau + 1 \right\}.$$

The Wasserstein-1 distance is given by

$$W_1^{(\tau)}(x_{1:T_x}, \{y_{1:T}^{(i)}\}_{i=1}^N) = \int_{\mathbb{R}} |F_{\tau}^g(x) - F_{\tau}^h(x)| dx. \quad (5)$$

We will calculate the Wasserstein-1 distance of 1-, 5-, 20-, 100- and 200-day returns.

- High order moment scores: skewness and kurtosis. We calculate

$$\left| \text{skew}(x_{1:T_x}) - \frac{1}{N} \sum_{1 \leq i \leq N} \text{skew}(y_{1:T}^{(i)}) \right|$$

and

$$\left| \text{kurt}(x_{1:T_x}) - \frac{1}{N} \sum_{1 \leq i \leq N} \text{kurt}(y_{1:T}^{(i)}) \right|$$

as the scores of skewness and kurtosis.

- Correlation scores. We look at the following four scores:
 - Autocorrelation of returns: $\text{ACF}_{\tau}(x_{1:T_x}) = \text{corr}(x_t, x_{t+\tau})$
 - Autocorrelation of absolute returns: $\text{ACF}_{\tau}^{(\text{abs})}(x_{1:T_x}) = \text{corr}(|x_t|, |x_{t+\tau}|)$
 - Autocorrelation of squared returns: $\text{ACF}_{\tau}^{(\text{sq})}(x_{1:T_x}) = \text{corr}(x_t^2, x_{t+\tau}^2)$
 - Leverage effect: $\text{Lev}_{\tau}(x_{1:T_x}) = \text{corr}(x_t, x_{t+\tau}^2)$

Each score is calculated for lag $1 \leq \tau \leq \delta$. Then we calculate

$$\sqrt{\sum_{1 \leq \tau \leq \delta} \left(\text{score}_{\tau}(x_{1:T_x}) - \frac{1}{N} \sum_{1 \leq i \leq N} \text{score}_{\tau}(y_{1:T}^{(i)}) \right)^2}$$

where score stands for ACF, $\text{ACF}^{(\text{abs})}$, $\text{ACF}^{(\text{sq})}$ and Lev.

Those metrics do not participate in the loss functions of the GANs during training, so they are suitable to evaluate the samples generated from the GANs.

5.2 Training

After we have the real data $x_{1:T_x}$, we apply a rolling window of length l to get the real dataset $\{x_{t:t+l-1}\}_{t=1}^{T_x-l+1}$ for training.

One important stylized fact of the asset returns is that tails of their distributions are heavier than that of the normal distribution. However, we usually use the normal distribution as the random noise input of GANs. Thus it is a question whether GANs are able to generate heavy-tailed distributions given normal noise. In [39], the authors use the inverse Lambert transform to make the returns closer to the normal distribution such that GANs do not need to generate heavy tails. But in our experiments, we still use the original returns as the training data. We would like to show that the proposed GANs can learn to generate heavy tails by themselves even if they are given normal noise input.

We also test the case of adding the cumulative sum of the returns as additional channels to the input of the discriminator. The output from the generator is a sequence $y_{1:l}$. Then the augmented input to the discriminator is $\tilde{\mathbf{Y}} \in \mathbb{R}^{l \times 2}$ where

$$\tilde{Y}_{t,j} = \begin{cases} y_{t,j}, & \text{if } j = 1 \\ \sum_{i=1}^t y_{i,j}, & \text{if } j = 2. \end{cases}$$

In this way, the input of the discriminator includes not only the returns, but also the log-prices starting from 0. The additional cumulative sum feature is added so that the discriminator can observe the returns over large intervals by taking the difference of

the log-prices at two time points instead of taking the cumulative sum of the returns over long intervals.

In the rest of this section, we compare the performance of the proposed TAGAN and TTGAN with QuantGAN [39], which has shown good results for the S&P 500 index simulation using the temporal convolutional network [35]. The data channel is $d = 1$. The data length is $l = 128$ for TAGAN and TTGAN while $l = 127$ for QuantGAN. The RFS is $f = 127$ for each GAN. The number of layers in the generator is $L_1^G = L_2^G = 3$ for TAGAN and $L = 5$ for TTGAN. The number of hidden channels is 64 in TAGAN and TTGAN and is 80 in QuantGAN. We calculate $M = 512$ simulated paths of length $T = 2560$ for evaluation. In the correlation scores, we let $\delta = 250$ in accordance with [39]. The loss for training QuantGAN is the loss of the original GAN in Equation (1), as used in their paper. We use the loss functions of the WGAN-GP in Equation (2) to train TAGAN and TTGAN.

5.3 Simulation of the medium kurtosis data

To make a fair comparison with QuantGAN, we use the same data in the paper of QuantGAN [39], which is the S&P 500 index daily data from May 1, 2009 to Nov 30, 2018 with $T_x = 2414$. The skewness of the data is -0.4667 and the kurtosis is 4.0648.

We test TAGAN, TTGAN and QuantGAN with and without the additional cumulative sum feature. We only present the cases of good performance since not every case works. The selected results of the three GANs without the additional cumulative sum feature, as well as TTGAN with the additional cumulative sum feature, are shown in Table 3. Here is the summary of results:

- The performance of the four candidates in Table 3 are close to each other and the difference is not significant.
- The cumulative sum feature only improves the performance of TTGAN. This means the transformer is more suitable to process features of different scales than the convolutional network. With the help of the cumulative sum feature, TTGAN reduces the Wasserstein-1 distance score of 200-day returns, which agrees with the purpose of the additional cumulative sum feature.

scores	TAGAN	TTGAN (w/o cumsum)	TTGAN (w/ cumsum)	QuantGAN
$W_1^{(1)}$	4.569e-04	2.143e-04	3.319e-04	2.940e-04
$W_1^{(5)}$	9.764e-04	4.803e-04	7.367e-04	6.999e-04
$W_1^{(20)}$	2.677e-03	1.574e-03	2.234e-03	1.800e-03
$W_1^{(100)}$	3.363e-03	4.338e-03	3.311e-03	4.952e-03
$W_1^{(200)}$	1.016e-02	1.128e-02	7.281e-03	1.377e-02
skewness	5.284e-02	1.110e-01	1.752e-01	2.014e-01
kurtosis	5.248e-01	3.363e-01	1.237e-01	3.096e-01
ACF	3.450e-01	3.609e-01	3.628e-01	3.420e-01
ACF ^(abs)	3.799e-01	3.727e-01	3.552e-01	3.742e-01
ACF ^(sq)	3.300e-01	3.274e-01	3.238e-01	3.301e-01
Lev	3.248e-01	3.368e-01	3.376e-01	3.305e-01

Table 3: Scores of the S&P 500 index simulation given the medium kurtosis data from May 1, 2009 to Nov 30, 2018.

5.4 Simulation of the high kurtosis data

To further test the ability of the GANs to generate data with high (negative) skewness and high kurtosis, we also use the S&P 500 index daily data from May 1, 2009 to Dec

31, 2020 as the training data, which includes the drawdowns in 2020. The size of the dataset is $T_x = 2938$, the skewness is -0.8132 and the kurtosis is 15.1333.

We test TAGAN, TTGAN and QuantGAN for the dataset. For TAGAN and QuantGAN, no cumulative sum is used, while for TTGAN, we always use the cumulative sum feature. We also test TTGAN using batch normalization by default and its variant where we replace batch normalization with layer normalization [2]. Layer normalization normalizes the input values across the features, while batch normalization normalizes the input values across the batch dimension. The results are summarized in Table 4. The results of TAGAN, TTGAN with batch normalization and QuantGAN are further illustrated in Figure 11, 12 and 13. Here are the summary of the results:

- All the GANs perform well in fitting the distribution.
- Although layer normalization is more often used in the transformer architecture, we found that the layer normalization transformer fails to generate samples with high kurtosis in our tests.
- The convolution-based GANs, TAGAN and QuantGAN, are very sensitive to the autocorrelation curves, while TTGAN tends to smooth the autocorrelation curves. The fluctuations in the autocorrelation curves are likely to be caused by randomness in the market. The convolution-based GANs are preferred if we need to replicate the realization of randomness, while the transformer-based TTGAN is more suitable if we would like to filter out the randomness.

scores	TAGAN	TTGAN (BN)	TTGAN (LN)	QuantGAN
$W_1^{(1)}$	4.823e-04	4.907e-04	2.431e-04	2.605e-04
$W_1^{(5)}$	1.097e-03	1.525e-03	7.800e-04	9.530e-04
$W_1^{(20)}$	2.844e-03	4.963e-03	1.804e-03	2.840e-03
$W_1^{(100)}$	5.542e-03	8.432e-03	1.265e-02	6.347e-03
$W_1^{(200)}$	2.050e-02	1.774e-02	3.033e-02	1.797e-02
skewness	2.539e-01	4.883e-02	1.663e-01	3.870e-02
kurtosis	2.173e-01	2.121e-01	4.591e+00	5.674e-01
ACF	3.323e-01	4.067e-01	4.273e-01	3.437e-01
ACF ^(abs)	3.792e-01	3.465e-01	3.740e-01	3.647e-01
ACF ^(sq)	2.409e-01	2.496e-01	3.175e-01	2.415e-01
Lev	2.300e-01	2.957e-01	2.945e-01	2.319e-01

Table 4: Scores of the S&P 500 index simulation given the high kurtosis data from May 1, 2009 to Dec 31, 2020.

6 Simulation of the option surface

In this section, we show the numerical results of the proposed networks for the option surface simulation.

6.1 Formulation

Suppose we have N_K relative strikes

$$\mathcal{K} = \{K_1, K_1 + \Delta K, \dots, K_1 + (N_K - 1)\Delta K\}$$

and N_M maturities

$$\mathcal{M} = \{M_1, M_2, \dots, M_{N_M}\}.$$

Let $d = N_M \times N_K$. The real data is $\{\mathbf{x}_t \in \mathbb{R}^d\}_{t=1}^{T_x}$ with the elements $\mathbf{x}_t = (x_{t,j})_{j=1}^d$, where $x_{t,(j_1-1)N_M+j_2} = \ln \sigma_{t,(j_1-1)N_M+j_2}$ is the log-volatility at time t with the relative strike $K_{j_2} = K_1 + (j_2 - 1)\Delta K$ and the maturity M_{j_1} .

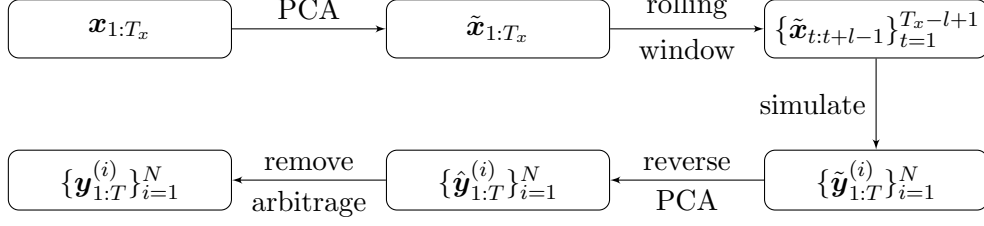


Figure 9: Pipeline of GANs using PCA.

6.2 Training

Having the real data $\mathbf{x}_{1:T_x} = \{\mathbf{x}_t\}_{t=1}^{T_x}$, we apply a rolling window of length l to get the dataset $\{\tilde{\mathbf{x}}_{t:t+l-1}\}_{t=1}^{T_x-l+1}$ for training. The output $\{\hat{\mathbf{y}}_{1:T}^{(i)}\}_{i=1}^N$ from the GAN generator is not guaranteed to be arbitrage-free. We apply the method in Appendix B to detect and remove arbitrage to obtain the arbitrage-free surface $\{\mathbf{y}_{1:T}^{(i)}\}_{i=1}^N$. In [38], the authors use the discrete local volatilities [7] to replace the implied volatilities when generating arbitrage-free option surfaces. The proposed networks are compatible with discrete local volatilities, but we still expect them to generate the implied volatilities and examine to what extent the outputs from the GANs violate the no-arbitrage condition.

The option volatility data is a high-dimensional data with high cross-correlation, so we could use principal component analysis (PCA) to reduce dimensionality. We perform PCA on the original data $\mathbf{x}_{1:T_x}$ and get the first \tilde{d} principal components $\{\tilde{\mathbf{x}}_t \in \mathbb{R}^{\tilde{d}}\}_{t=1}^{T_x}$. To be more specific, suppose the real data matrix $\mathbf{X} \in \mathbb{R}^{T_x \times d}$ is $\mathbf{X} = (\mathbf{x}_1, \mathbf{x}_2, \dots, \mathbf{x}_{T_x})^\top$. We get its singular value decomposition (SVD) as $\mathbf{X} = \mathbf{U}\mathbf{D}\mathbf{V}^\top$, and then take the first \tilde{d} columns of \mathbf{U} to be the principal components, i.e. $\mathbf{U}_{:,1:\tilde{d}} = (\tilde{\mathbf{x}}_1, \tilde{\mathbf{x}}_2, \dots, \tilde{\mathbf{x}}_{T_x})^\top$. Next, we apply a rolling window of length l to get the real dataset $\{\tilde{\mathbf{x}}_{t:t+l-1}\}_{t=1}^{T_x-l+1}$ for training. The GAN generator is responsible for generating the first \tilde{d} principal components $\{\tilde{\mathbf{y}}_{1:T}^{(i)}\}_{i=1}^N$, and they are used to recover the log-volatility surfaces $\{\hat{\mathbf{y}}_{1:T}^{(i)}\}_{i=1}^N$ through reverse PCA, where $\hat{\mathbf{y}}_t^{(i)} = \mathbf{V}_{:,1:\tilde{d}} \mathbf{D}_{1:\tilde{d},1:\tilde{d}} \tilde{\mathbf{y}}_t^{(i)}$. Finally we apply the method in Appendix B to get the arbitrage-free surfaces $\{\mathbf{y}_{1:T}^{(i)}\}_{i=1}^N$. This process is summarized in Figure 9.

Since we find it is helpful to include both returns and log-prices in the S&P 500 index simulation, we think it could also be helpful when the differences of the log-volatilities (called log-volatility returns hereafter) are used as the additional feature. The output from the generator is a sequence $\hat{\mathbf{y}}_{1:l}$. Then the augmented input to the discriminator is $\bar{\mathbf{Y}} \in \mathbb{R}^{l \times 2d}$ where

$$\bar{Y}_{t,j} = \begin{cases} \hat{y}_{t,j}, & \text{if } 1 \leq j \leq d \\ \hat{y}_{t,j-d} - \hat{y}_{t-1,j-d}, & \text{if } 2 \leq t \leq l \text{ and } d+1 \leq j \leq 2d \\ 0, & \text{if } t=1 \text{ and } d+1 \leq j \leq 2d. \end{cases}$$

In this way, the input of the discriminator includes both the log-volatilities and the log-volatility returns.

To summarize, we have three choices to train the GANs:

- Use the log-volatility surfaces as the real data. The generators simulate the log-volatility surfaces.
- Use the principal components of log-volatility surfaces as the real data. The generators simulate the principal components.
- Use the log-volatility surfaces and their returns as the real data. The generators simulate the log-volatility surfaces.

6.3 Stylized facts and metrics

Here are some stylized facts of the option surface summarized in [40].

- The volatility smile. Deep in-the-money and out-of-the-money volatility are generally higher than at-the-money volatility.
- Volatilities have high serial autocorrelation.
- Volatilities show high cross-correlation. The correlation matrix of the log-volatilities of different relative strikes and maturities in the S&P 500 index option data in Section 6.4 is shown in Figure 10. Higher cross-correlation is observed for proximate relative strikes and maturities. Volatilities of longer maturities have higher cross-correlation than volatilities of shorter maturities.

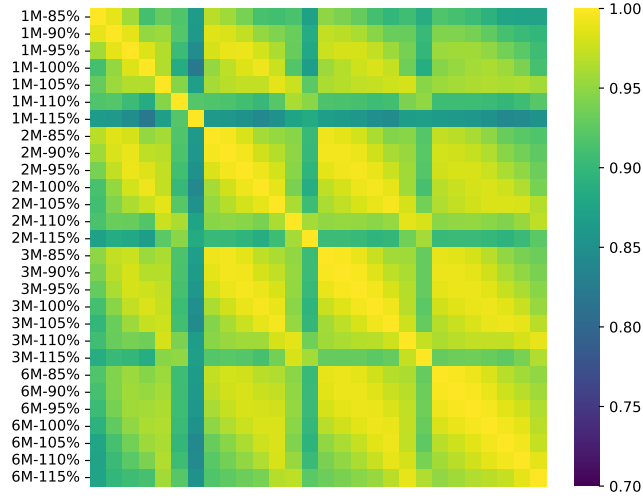


Figure 10: Cross-correlation matrix of the log-volatilities of the S&P 500 index options. The label means ‘maturity - relative strike’.

Based on the stylized facts, the evaluation metrics are listed as follows:

- The Wasserstein-1 distance of distribution of volatilities

$$\frac{1}{d} \sum_{j=1}^d W_1^{(1)} \left(\{x_{t,j}\}_{t=1}^{T_x}, \{\{y_{t,j}^{(i)}\}_{t=1}^T\}_{i=1}^N \right)$$

where the Wasserstein-1 distance is already defined in Equation (5).

- High order moment scores of skewness

$$\frac{1}{d} \sum_{j=1}^d \left| \text{skew}(x_{1:T_x,j}) - \frac{1}{N} \sum_{1 \leq i \leq N} \text{skew}(y_{1:T,j}^{(i)}) \right|$$

and kurtosis

$$\frac{1}{d} \sum_{j=1}^d \left| \text{kurt}(x_{1:T_x,j}) - \frac{1}{N} \sum_{1 \leq i \leq N} \text{kurt}(y_{1:T,j}^{(i)}) \right|.$$

- Autocorrelation score of the series and returns. Define

$$\text{ACF}_\tau^{(r)}(x_{1:T_x}) = \text{ACF}_\tau(x_{2:T_x} - x_{1:T_x-1}).$$

We calculate

$$\frac{1}{d} \sum_{j=1}^d \sqrt{\sum_{1 \leq \tau \leq \delta} \left(\text{score}_\tau(x_{1:T_x,j}) - \frac{1}{N} \sum_{1 \leq i \leq N} \text{score}_\tau(y_{1:T,j}^{(i)}) \right)^2}$$

where score stands for ACF and $\text{ACF}^{(r)}$.

- Cross-correlation score. Let $\Sigma_{\mathbf{x}} \in \mathbb{R}^{d \times d}$ be the cross-correlation matrix of $\{\mathbf{x}_t, 1 \leq t \leq T_x\}$ and $\Sigma_{\mathbf{y}} \in \mathbb{R}^{d \times d}$ be the cross-correlation matrix of $\{\mathbf{y}_t^{(i)}, 1 \leq t \leq T_x, 1 \leq i \leq N\}$. Then the score is defined to the Frobenius norm of the difference $\|\Sigma_{\mathbf{x}} - \Sigma_{\mathbf{y}}\|_F$.
- Arbitrage rate. The score is calculated as the percentage of the outputs from the GANs $\hat{\mathbf{y}}_{1:T}^{(i)}$ that violate the no-arbitrage condition

$$\#\{(i, t) : \hat{\mathbf{y}}_t^{(i)} \text{ that violates the no-arbitrage condition}, 1 \leq i \leq N, 1 \leq t \leq T\} / (NT).$$

This is a score that shows how well the GAN can learn the no-arbitrage condition.

6.4 Data and results

We use the daily data of the S&P 500 index options from Jan 02, 2009 to Oct 30, 2020 as the real data. The maturities are

$$\mathcal{M} = \{1\text{-month}, 2\text{-month}, 3\text{-month}, 6\text{-month}\}$$

and the relative strikes are

$$\mathcal{K} = \{85\%, 90\%, 95\%, 100\%, 105\%, 110\%, 115\%\}.$$

The data channel is $d = 28$ and the sequence length is $T_x = 2979$.

We compare the performance of the proposed TAGAN and TTGAN with QuantGAN [39] and try both PCA and the additional log-volatility return feature. The data length is $l = 128$ for TAGAN and TTGAN while $l = 127$ for QuantGAN. The RFS is $f = 383$ for each GAN. We let $\tilde{d} = 10$ for PCA. The number of layers in the generator is $L_1^G = L_2^G = 3$ for TAGAN and $L = 5$ for TTGAN. The number of hidden channels is 64 in TAGAN and TTGAN and is 80 in QuantGAN. We calculate $M = 512$ simulated paths of length $T = 2560$ for evaluation. In the correlation scores, we let $\delta = 64$. The loss for training QuantGAN is the loss of the original GAN in Equation (1). We use the loss functions of the WGAN-GP in Equation (2) to train TAGAN and TTGAN.

The results of TAGAN with and without PCA, TTGAN with and without the return feature, and QuantGAN, are summarized in Table 5. The good candidates, which are TAGAN with PCA, TTGAN with the return feature, and QuantGAN are further illustrated in Figure 14, 15 and 16. Here are some key points of results:

- Only TTGAN is improved by the additional return feature. It is not a surprise to see TTGAN can accept the additional return feature, since it accepts both log-prices and log returns for the S&P 500 index simulation. The additional return feature improves the score of autocorrelation and cross-correlation, and facilitates the GAN to learn the no-arbitrage condition.
- Only TAGAN is improved by PCA. If a GAN is able to generate option surfaces by means of principle components, that will significantly reduce the score of cross-correlation and reduce the rate that the output needs to be modified by the no-arbitrage condition.
- In Figure 17, we show examples of autocorrelation of log-volatility returns from the three GANs. There are huge fluctuations in the autocorrelation of QuantGAN. Also, some fluctuations are observed at the small time lags in the autocorrelation of TAGAN. In contrast, the autocorrelation of TTGAN is flat. It means the attention layer is better at generating sequences with smooth autocorrelation, which matches the results of the S&P 500 index simulation.

7 Conclusion

In this paper, we first define the generative model of time series, distinguish it from the generator of fixed dimension distributions. We then propose two GANs, the temporal attention GAN and the temporal transformer GAN, based on the causal attention

scores	TAGAN	TAGAN	TTGAN	TTGAN	QuantGAN
	(w/o PCA)	(w/ PCA)	(w/o returns)	(w/ returns)	
$W_1^{(1)}$	1.788e-02	1.651e-02	1.239e-02	1.512e-02	1.355e-02
skewness	2.434e-01	2.450e-01	2.077e-01	8.204e-02	8.560e-02
kurtosis	6.052e-01	2.710e-01	5.212e-01	5.607e-01	4.065e-01
ACF	3.065e-01	3.444e-01	4.359e-01	1.845e-01	1.754e-01
ACF ^(r)	3.601e-01	2.580e-01	3.727e-01	2.667e-01	8.683e-01
cross-corr	4.883e-01	1.016e-01	6.027e-01	2.618e-01	2.284e-01
arbitrage rate	30.10%	1.55%	21.16%	8.88%	12.86%

Table 5: Scores of the S&P 500 index option surface simulation.

layer, which is able to increase the receptive field size without introducing more parameters. We have successfully trained the temporal transformer GAN using around 3000 samples of financial time series with the help of sparse attention, despite the fact that both GANs and transformers are notoriously known for being difficult to train.

In the numerical experiments, we compare the two proposed GANs with **QuantGAN** for the stock index and option surface simulation and evaluate the results with the scores based on the stylized facts. The proposed GANs are able to replicate the distribution, the heavy tails and the long-range dependencies, as well as the cross-correlation in the multivariate case. Specifically, the attention-based GANs show the following advantages:

- The **TTGAN** tends to generate smoother autocorrelation of returns. However, the convolution-based **QuantGAN** tends to overfit autocorrelation curves. For option surface simulation, the **QuantGAN** even fails to replicate the autocorrelation of volatility returns. The **TAGAN**, as a mixture of convolutions and attention, lies between **TTGAN** and **QuantGAN**.
- The transformer discriminator in **TTGAN** is more flexible such that it can accept both level and return features. We can make use of its ability to process features of different scales to improve the performance of GANs.
- The **TAGAN** is able to learn and generate samples in the space of principal components, which makes it possible to simulate time series in higher-dimensional spaces utilizing PCA.
- The receptive field size of the attention-based GANs is not bounded by the number of parameters or the network depth. This is useful especially when the size of real data is limited and a large number of parameters would lead to overfitting.

The generative models discussed in the paper are all unconditional models, which generate time series given noise series. In the future, it would be interesting to compare the performance of unconditional models and conditional models, which generate future time series given noise as well as historical time series. The conditional models are trickier for the following reasons:

- The conditional models need to learn the conditional distribution given history time series, which is generally more complex than the unconditional distribution.
- The input of the unconditional model is random noise generated during training. Thus, the unconditional model would not memorize the input. However, the conditional model can easily remember real data and perform extremely well when real data is used as the condition input. When the conditional model uses the time series generated by itself as the condition input and tries to prolong the generated time series, its performance could be much worse. For that reason, we need additional techniques to deal with overfitting.

References

- [1] M. Arjovsky, S. Chintala, and L. Bottou. Wasserstein GAN. *arXiv:1701.07875*, Dec. 2017. arXiv: 1701.07875.
- [2] J. L. Ba, J. R. Kiros, and G. E. Hinton. Layer normalization. *arXiv preprint arXiv:1607.06450*, 2016.
- [3] D. Bahdanau, K. Cho, and Y. Bengio. Neural machine translation by jointly learning to align and translate. *arXiv preprint arXiv:1409.0473*, 2014.
- [4] F. Black and M. Scholes. The pricing of options and corporate liabilities. *Journal of Political Economy*, 81(3):637–654, 1973.
- [5] T. Bollerslev. Generalized autoregressive conditional heteroskedasticity. *Journal of Econometrics*, 31(3):307–327, Apr. 1986.
- [6] A. Brock, J. Donahue, and K. Simonyan. Large scale GAN training for high fidelity natural image synthesis. *arXiv preprint arXiv:1809.11096*, 2018.
- [7] H. Buehler and E. Ryskin. Discrete local volatility for large time steps (extended version). *Available at SSRN 2642630*, 2017.
- [8] Z. Che, S. Purushotham, G. Li, B. Jiang, and Y. Liu. Hierarchical deep generative models for multi-rate multivariate time series. In *International Conference on Machine Learning*, pages 784–793, 2018.
- [9] R. Child, S. Gray, A. Radford, and I. Sutskever. Generating long sequences with sparse transformers. *arXiv preprint arXiv:1904.10509*, 2019.
- [10] J. Chung, C. Gulcehre, K. Cho, and Y. Bengio. Empirical evaluation of gated recurrent neural networks on sequence modeling. *arXiv preprint arXiv:1412.3555*, 2014.
- [11] R. Cont. Empirical properties of asset returns: stylized facts and statistical issues. *Quantitative Finance*, 1(2):223–236, feb 2001.
- [12] G. Daras, A. Odena, H. Zhang, and A. G. Dimakis. Your local GAN: Designing two dimensional local attention mechanisms for generative models. In *Proceedings of the IEEE/CVF Conference on Computer Vision and Pattern Recognition (CVPR)*, June 2020.
- [13] F. De Meer Pardo. *Enriching Financial Datasets with Generative Adversarial Networks*. PhD thesis, Master’s thesis, Delft University of Technology, the Netherlands, 2019.
- [14] C. Esteban, S. L. Hyland, and G. Rätsch. Real-valued (medical) time series generation with recurrent conditional gans. *arXiv preprint arXiv:1706.02633*, 2017.
- [15] R. Fu, J. Chen, S. Zeng, Y. Zhuang, and A. Sudjianto. Time series simulation by conditional generative adversarial net. *arXiv preprint arXiv:1904.11419*, 2019.
- [16] I. Goodfellow, J. Pouget-Abadie, M. Mirza, B. Xu, D. Warde-Farley, S. Ozair, A. Courville, and Y. Bengio. Generative adversarial nets. In *Advances in Neural Information Processing Systems*, volume 27. Curran Associates, Inc., 2014.
- [17] I. Gulrajani, F. Ahmed, M. Arjovsky, V. Dumoulin, and A. C. Courville. Improved Training of Wasserstein GANs. In *Advances in Neural Information Processing Systems*, volume 30. Curran Associates, Inc., 2017.
- [18] K. He, X. Zhang, S. Ren, and J. Sun. Deep residual learning for image recognition. In *Proceedings of the IEEE Conference on Computer Vision and Pattern Recognition (CVPR)*, June 2016.
- [19] S. L. Heston. A closed-form solution for options with stochastic volatility with applications to bond and currency options. *The review of financial studies*, 6(2):327–343, 1993.
- [20] S. Hochreiter and J. Schmidhuber. Long short-term memory. *Neural computation*, 9(8):1735–1780, 1997.

- [21] M. Hofert, A. Prasad, and M. Zhu. Multivariate time-series modeling with generative neural networks. *Econometrics and Statistics*, 23:147–164, 2022.
- [22] D. A. Hudson and L. Zitnick. Generative adversarial transformers. In *Proceedings of the 38th International Conference on Machine Learning*, volume 139 of *Proceedings of Machine Learning Research*, pages 4487–4499. PMLR, 18–24 Jul 2021.
- [23] S. Ioffe and C. Szegedy. Batch normalization: Accelerating deep network training by reducing internal covariate shift. In *Proceedings of the 32nd International Conference on Machine Learning*, volume 37 of *Proceedings of Machine Learning Research*, pages 448–456, Lille, France, 07–09 Jul 2015. PMLR.
- [24] Y. Jiang, S. Chang, and Z. Wang. TransGAN: Two Pure Transformers Can Make One Strong GAN, and That Can Scale Up. In *Advances in Neural Information Processing Systems*, volume 34, pages 14745–14758. Curran Associates, Inc., 2021.
- [25] A. Kondratyev and C. Schwarz. The market generator. *Available at SSRN 3384948*, 2019.
- [26] A. Koochali, P. Schichtel, A. Dengel, and S. Ahmed. Probabilistic Forecasting of Sensory Data With Generative Adversarial Networks – ForGAN. *IEEE Access*, 7:63868–63880, 2019.
- [27] A. Koshiyama, N. Firoozye, and P. Treleaven. Generative adversarial networks for financial trading strategies fine-tuning and combination. *Quantitative Finance*, pages 1–17, Sept. 2020.
- [28] Y. LeCun, B. Boser, J. S. Denker, D. Henderson, R. E. Howard, W. Hubbard, and L. D. Jackel. Backpropagation Applied to Handwritten Zip Code Recognition. *Neural Computation*, 1(4):541–551, Dec. 1989.
- [29] M.-T. Luong, H. Pham, and C. D. Manning. Effective approaches to attention-based neural machine translation. *arXiv preprint arXiv:1508.04025*, 2015.
- [30] D. B. Madan and E. Seneta. The variance gamma (VG) model for share market returns. *Journal of business*, pages 511–524, 1990.
- [31] T. Miyato, T. Kataoka, M. Koyama, and Y. Yoshida. Spectral normalization for generative adversarial networks. *arXiv preprint arXiv:1802.05957*, 2018.
- [32] O. Mogren. C-rnn-gan: Continuous recurrent neural networks with adversarial training. *arXiv preprint arXiv:1611.09904*, 2016.
- [33] H. Ni, L. Szpruch, M. Wiese, S. Liao, and B. Xiao. Conditional Sig-Wasserstein GANs for Time Series Generation. *arXiv:2006.05421*, June 2020. arXiv: 2006.05421.
- [34] S. Takahashi, Y. Chen, and K. Tanaka-Ishii. Modeling financial time-series with generative adversarial networks. *Physica A: Statistical Mechanics and its Applications*, 527:121261, Aug. 2019.
- [35] A. van den Oord, S. Dieleman, H. Zen, K. Simonyan, O. Vinyals, A. Graves, N. Kalchbrenner, A. Senior, and K. Kavukcuoglu. WaveNet: A Generative Model for Raw Audio. In *Proc. 9th ISCA Workshop on Speech Synthesis Workshop (SSW 9)*, page 125, 2016.
- [36] A. Vaswani, N. Shazeer, N. Parmar, J. Uszkoreit, L. Jones, A. N. Gomez, L. u. Kaiser, and I. Polosukhin. Attention is all you need. In *Advances in Neural Information Processing Systems*, volume 30. Curran Associates, Inc., 2017.
- [37] C. Villani. *Optimal transport: old and new*, volume 338. Springer, 2009.
- [38] M. Wiese, L. Bai, B. Wood, and H. Buehler. Deep hedging: Learning to simulate equity option markets. *arXiv preprint arXiv:1911.01700*, 2019.
- [39] M. Wiese, R. Knobloch, R. Korn, and P. Kretschmer. Quant GANs: deep generation of financial time series. *Quantitative Finance*, 20(9):1419–1440, Sept. 2020.
- [40] M. Wiese, B. Wood, A. Pachoud, R. Korn, H. Buehler, P. Murray, and L. Bai. Multi-asset spot and option market simulation. *arXiv preprint arXiv:2112.06823*, 2021.

- [41] J. Yoon, D. Jarrett, and M. van der Schaar. Time-series generative adversarial networks. In *Advances in Neural Information Processing Systems*, volume 32. Curran Associates, Inc., 2019.
- [42] H. Zhang, I. Goodfellow, D. Metaxas, and A. Odena. Self-attention generative adversarial networks. In *Proceedings of the 36th International Conference on Machine Learning*, volume 97 of *Proceedings of Machine Learning Research*, pages 7354–7363. PMLR, 09–15 Jun 2019.
- [43] K. Zhang, G. Zhong, J. Dong, S. Wang, and Y. Wang. Stock Market Prediction Based on Generative Adversarial Network. *Procedia Computer Science*, 147:400–406, 2019.
- [44] X. Zhou, Z. Pan, G. Hu, S. Tang, and C. Zhao. Stock Market Prediction on High-Frequency Data Using Generative Adversarial Nets. *Mathematical Problems in Engineering*, 2018:1–11, 2018.

A Numerical experiment results

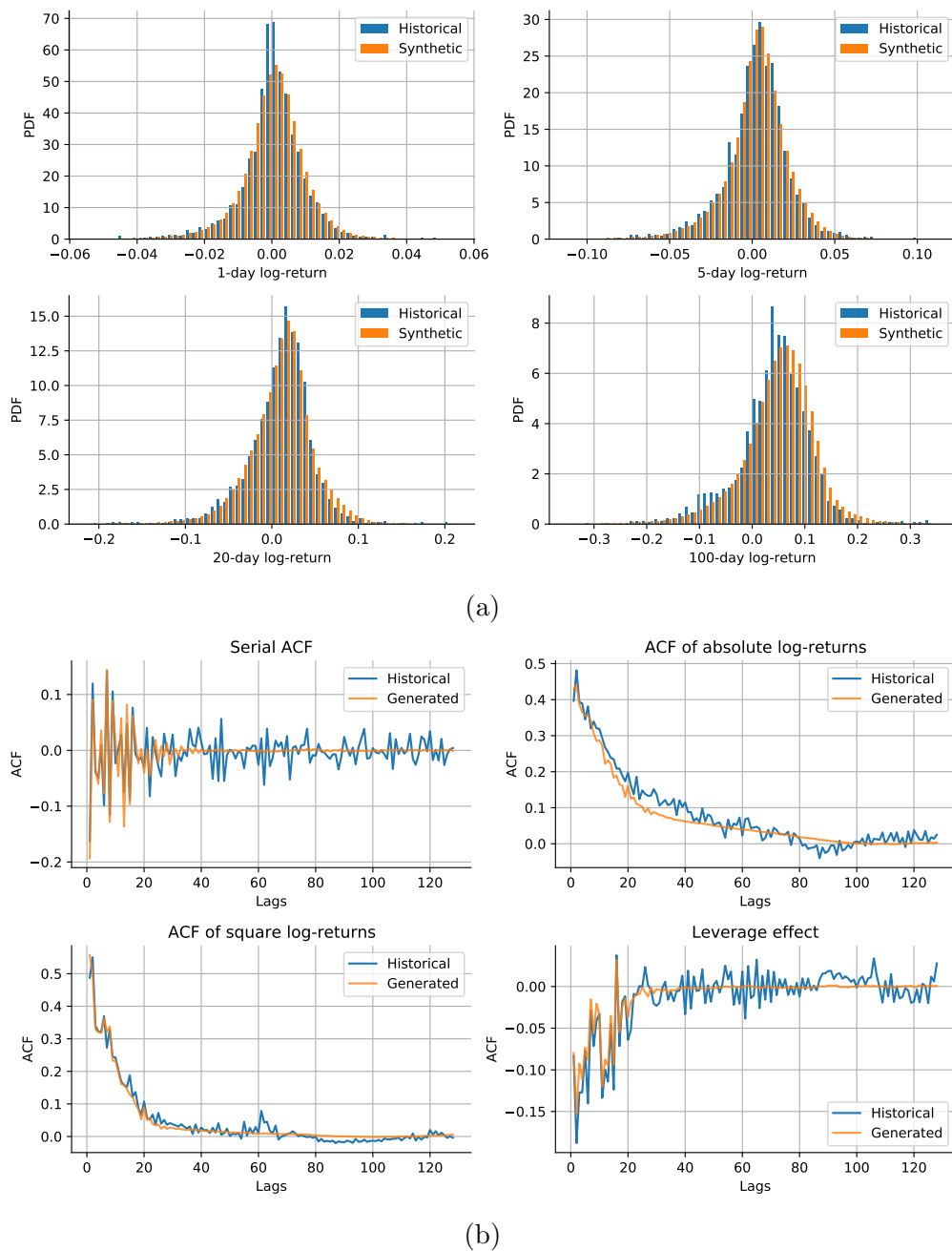
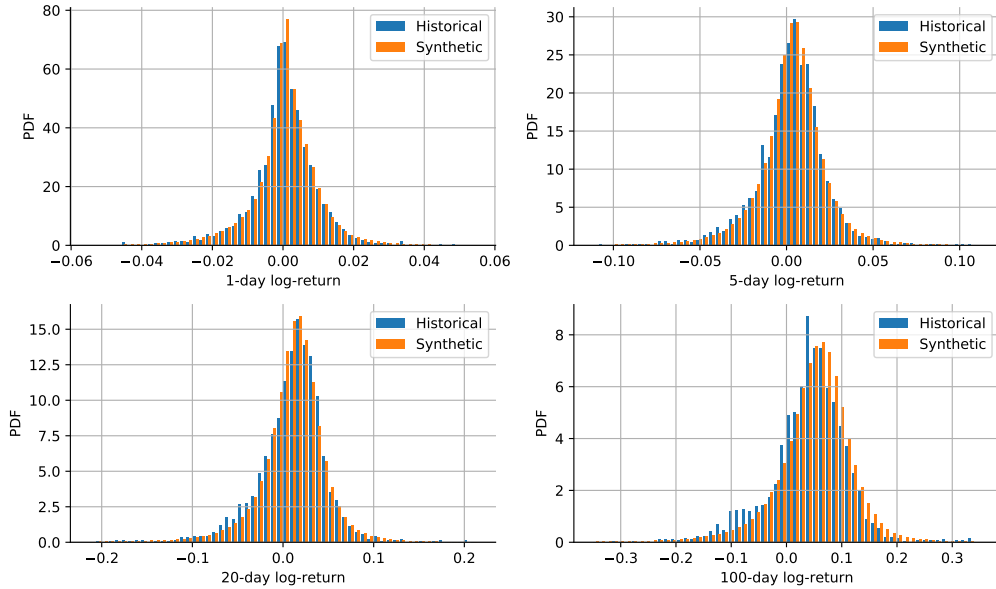
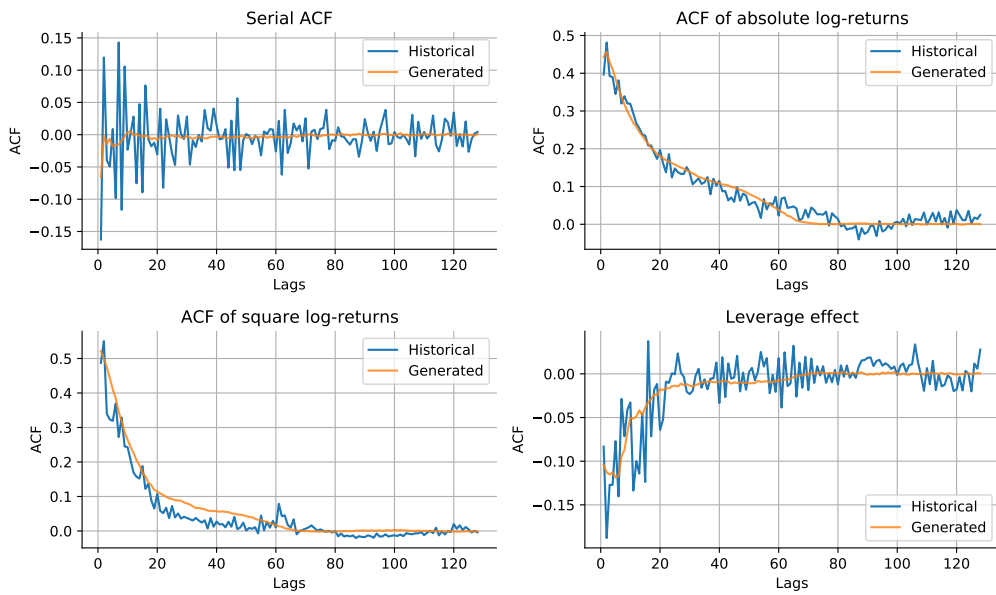


Figure 11: TAGAN simulation results of the S&P 500 index. (a) Comparison of the generated and historical densities of log returns. (b) Comparison of the generated mean autocorrelation and historical autocorrelation of daily log returns.

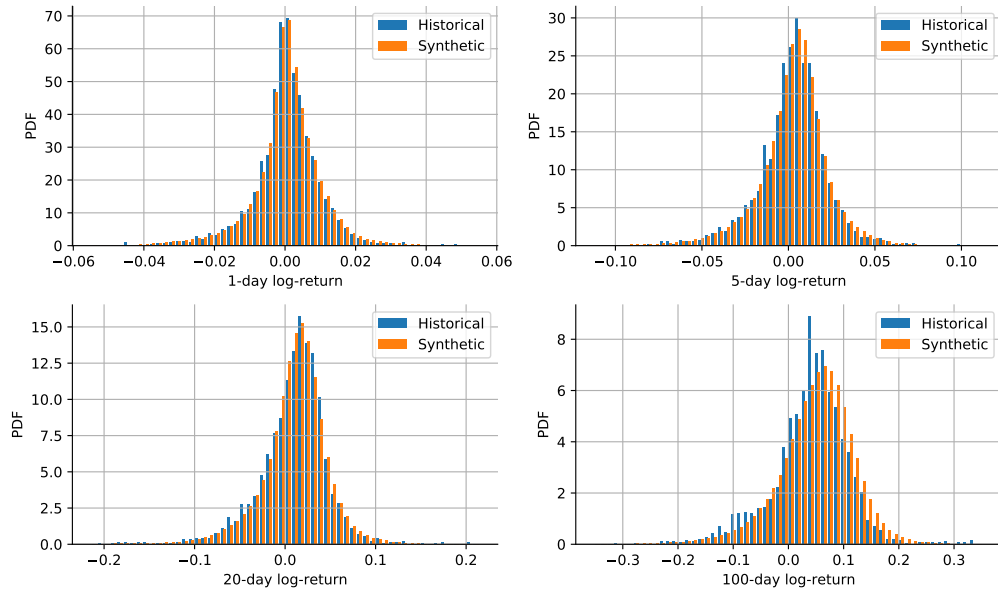


(a)

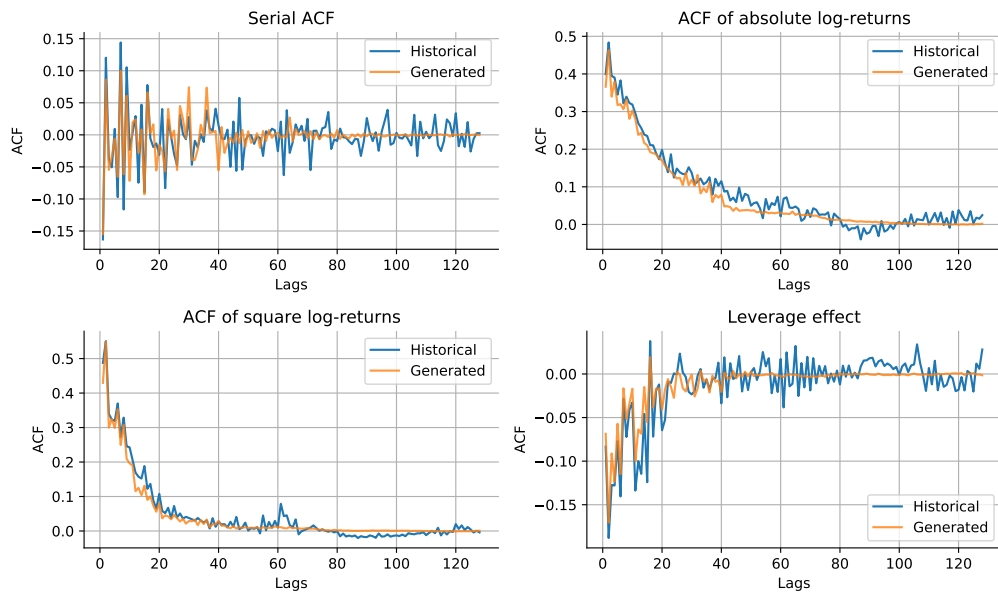


(b)

Figure 12: TTGAN simulation results of the S&P 500 index. (a) Comparison of the generated and historical densities of log returns. (b) Comparison of the generated mean autocorrelation and historical autocorrelation of daily log returns.

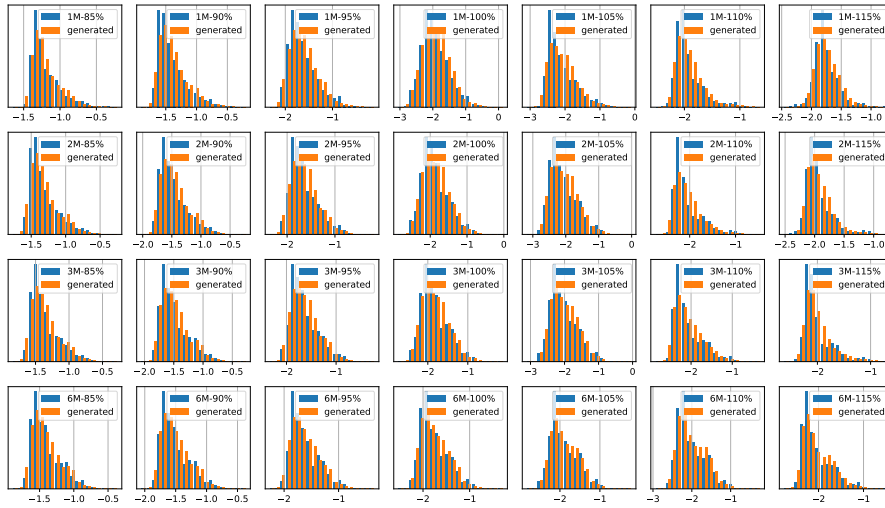


(a)

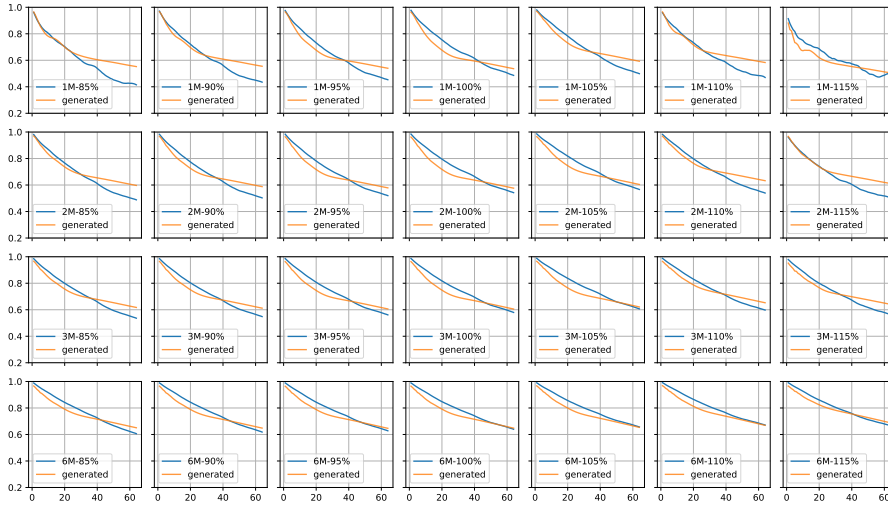


(b)

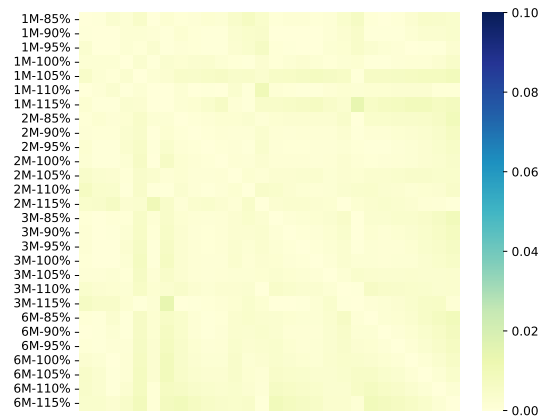
Figure 13: QuantGAN simulation results of the S&P 500 index. (a) Comparison of the generated and historical densities of log returns. (b) Comparison of the generated mean autocorrelation and historical autocorrelation of daily log returns.



(a)

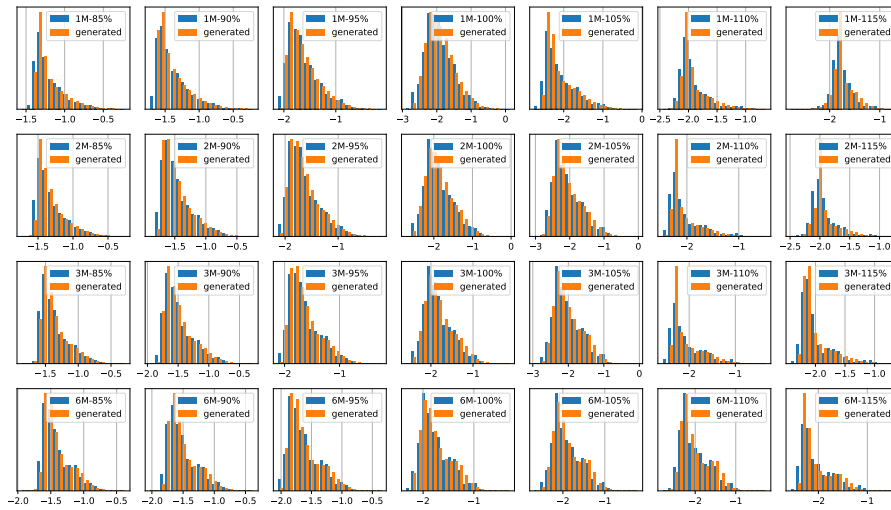


(b)

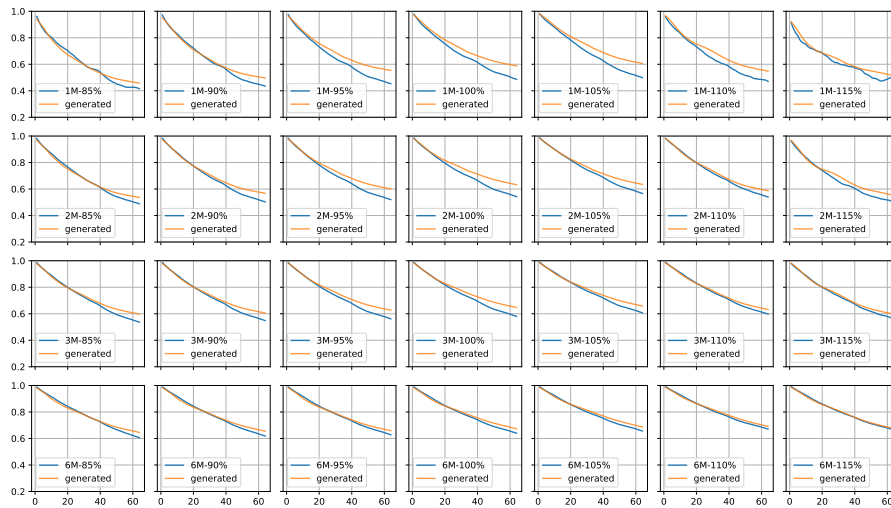


(c)

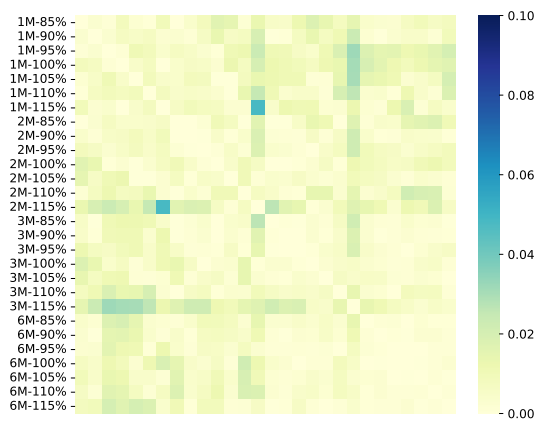
Figure 14: TAGAN simulation results of the S&P 500 index options. (a) Comparison of the generated and historical densities of log-volatilities. (b) Comparison of the generated mean autocorrelation and historical autocorrelation of log-volatilities. (c) Difference of the generated and historical cross-correlation of log-volatilities $|\Sigma_{\mathbf{x}} - \Sigma_{\mathbf{y}}|$.



(a)

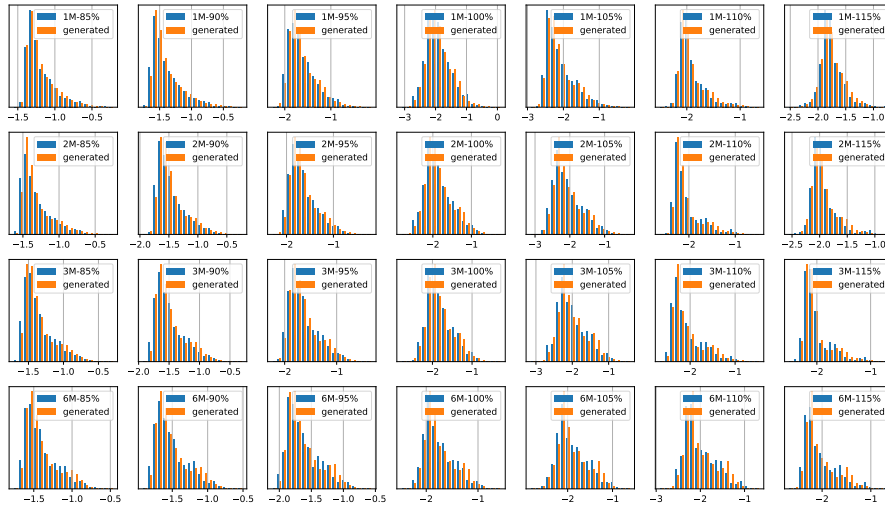


(b)

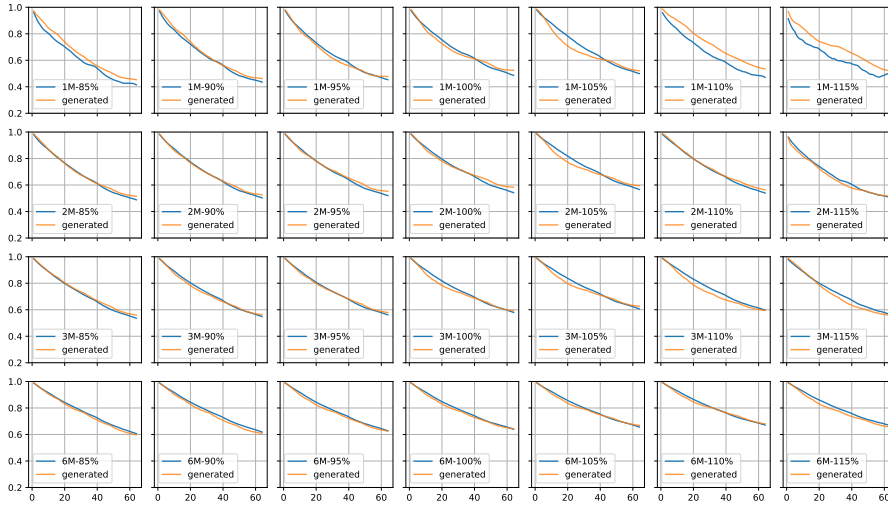


(c)

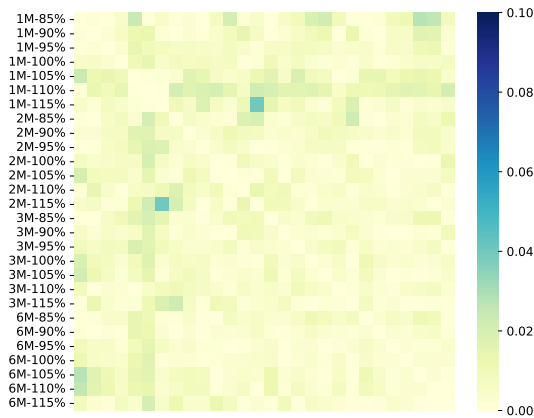
Figure 15: TTGAN simulation results of the S&P 500 index options. (a) Comparison of the generated and historical densities of log-volatilities. (b) Comparison of the generated mean autocorrelation and historical autocorrelation of log-volatilities. (c) Difference of the generated and historical cross-correlation of log-volatilities $|\Sigma_{\mathbf{x}} - \Sigma_{\mathbf{y}}|$.



(a)



(b)



(c)

Figure 16: **QuantGAN** simulation results of the S&P 500 index options. (a) Comparison of the generated and historical densities of log-volatilities. (b) Comparison of the generated mean autocorrelation and historical autocorrelation of log-volatilities. (c) Difference of the generated and historical cross-correlation of log-volatilities $|\Sigma_x - \Sigma_y|$.

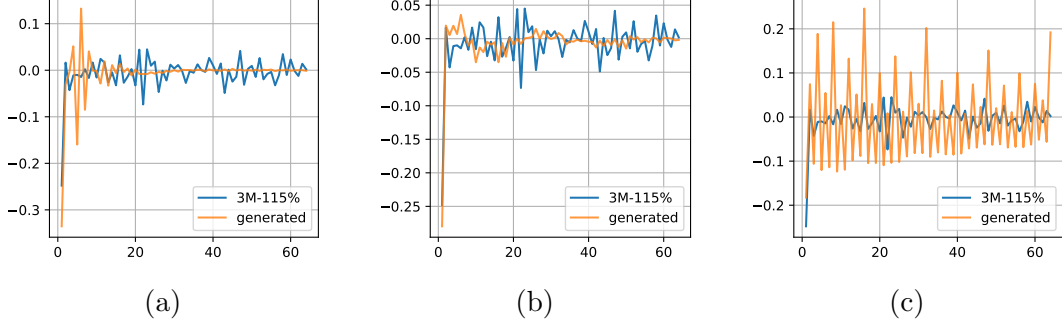


Figure 17: Example of the generated mean autocorrelation and historical autocorrelation of log-volatility returns of the S&P 500 index options. (a) TAGAN. (b) TTGAN. (c) QuantGAN.

B Arbitrage-free option surface

In [7], the authors give the condition that a call option surface is arbitrage-free. Suppose we have the set of relative strikes

$$\mathcal{K} = \{K_0, K_1, K_2, \dots, K_{N_K}, K_{N_K+1}\}$$

where $K_i < K_{i+1}, 0 \leq i \leq N_K$ and the set of maturities

$$\mathcal{M} = \{M_1, M_2, \dots, M_{N_M}\}$$

where $M_j < M_{j+1}, 1 \leq j \leq N_M - 1$. Let $C_{i,j}$ be the call price at strike K_i and maturity M_j . K_0 is sufficiently small and K_{N_K+1} is sufficiently large, so that we have $C_{0,j} = 1 - K_0$ and $C_{N_K+1,j} = 0$. Then the variables $\{C_{i,j}, 1 \leq i \leq N_K, 1 \leq j \leq N_M\}$ need to satisfy the following conditions:

$$\begin{cases} C_{1,j} \geq 1 - K_1, & \forall 1 \leq j \leq N_M \\ C_{N_K,j} \geq 0, & \forall 1 \leq j \leq N_M \\ C_{i,j} \geq C_{i,j-1}, & \forall 1 \leq i \leq N_K, 2 \leq j \leq N_M \\ \frac{C_{i,j} - C_{i-1,j}}{K_i - K_{i-1}} \leq \frac{C_{i+1,j} - C_{i,j}}{K_{i+1} - K_i}, & \forall 1 \leq i \leq N_K, 1 \leq j \leq N_M \end{cases} \quad (6)$$

Suppose $\{\hat{C}_{i,j}, 1 \leq i \leq N_K, 1 \leq j \leq N_M\}$ is the call option surface that does not satisfy the conditions, we use the following linear programming to solve the closest arbitrage-free surface.

$$\min_{C_{i,j}, 1 \leq i \leq N_K, 1 \leq j \leq N_M} \sum_{i=1}^{N_K} \sum_{j=1}^{N_M} |\hat{C}_{i,j} - C_{i,j}|$$

such that the constraints in (6) are satisfied.

If we start from the volatility surface, we calculate the call options and detect any violations of the constraints in (6). If so, we perform the linear programming to remove the arbitrages and calculate the corrected implied volatilities.

C Losses of GANs

In [16], the authors proposed the original loss of GANs:

$$\min_{\theta_G} \max_{\theta_D} \mathbb{E}_{\mathbf{X}} \ln(D(\mathbf{X}; \theta_D)) + \mathbb{E}_{\mathbf{Z}} \ln(1 - D(G(\mathbf{Z}; \theta_G); \theta_D))$$

where the discriminator is $D(\cdot; \theta_D) : \mathbb{R}^{l \times d} \rightarrow (0, 1)$ and the output of the discriminator stands for the probability that its input is considered real data. Thus the losses for

the generator and the discriminator are

$$\begin{aligned} & \min_{\theta_G} \mathbb{E}_{\mathbf{Z}} \ln(1 - D(G(\mathbf{Z}; \theta_G); \theta_D)) \\ & \min_{\theta_D} -\mathbb{E}_{\mathbf{X}} \ln(D(\mathbf{X}; \theta_D)) - \mathbb{E}_{\mathbf{Z}} \ln(1 - D(G(\mathbf{Z}; \theta_G); \theta_D)) \end{aligned}$$

respectively. In practice, $D(G(\mathbf{Z}; \theta_G); \theta_D)$ is close to 0 in the beginning since the generator has not learned anything. The gradient of $\ln(1 - D(G(\mathbf{Z}; \theta_G); \theta_D))$ is small and convergence would be slow. So the loss for the generator is replaced with

$$\min_{\theta_G} -\mathbb{E}_{\mathbf{Z}} \ln(D(G(\mathbf{Z}; \theta_G); \theta_D)).$$

In this paper, we use the discriminator $D(\cdot; \theta_D) : \mathbb{R}^{l \times d} \rightarrow \mathbb{R}$ to include the case of WGAN-GP. So the sigmoid function $\sigma(D(\cdot; \theta_D))$ stands for the probability. Thus the original losses of GANs are written as

$$\begin{aligned} & \min_{\theta_G} \mathbb{E}_{\mathbf{Z}} -\ln(\sigma(D(G(\mathbf{Z}; \theta_G); \theta_D))) \\ & \min_{\theta_D} \mathbb{E}_{\mathbf{X}, \mathbf{Z}} -\ln(\sigma(D(\mathbf{X}; \theta_D))) - \ln(1 - \sigma(D(G(\mathbf{Z}; \theta_G); \theta_D))). \end{aligned}$$

The Wasserstein GAN in [1] approaches the loss of GANs in a different way. It tries to minimize the Wasserstein-1 distance between the real distribution and the generated distribution:

$$W(\mathbb{P}_r, \mathbb{P}_g) = \inf_{\gamma \in \Pi(\mathbb{P}_r, \mathbb{P}_g)} \mathbb{E}_{(\mathbf{X}, \mathbf{Y}) \sim \gamma} \|\mathbf{X} - \mathbf{Y}\|$$

where \mathbb{P}_r is the real distribution of \mathbf{X} and \mathbb{P}_g is the generated distribution of $G(\mathbf{Z}; \theta_G)$, and $\Pi(\mathbb{P}_r, \mathbb{P}_g)$ denotes the set of all joint distributions γ whose marginals are respectively \mathbb{P}_r and \mathbb{P}_g . $\|\cdot\|$ is the Frobenius norm. Then they make use of the Kantorovich-Rubinstein duality [37] to get

$$W(\mathbb{P}_r, \mathbb{P}_g) = \sup_{\|f\|_L \leq 1} \mathbb{E}_{\mathbf{X}} f(\mathbf{X}) - \mathbb{E}_{\mathbf{Z}} f(G(\mathbf{Z}; \theta_G))$$

where $\|f\|_L \leq 1$ means the 1-Lipschitz function f . For a differentiable f , this means $\|\nabla f\| \leq 1$. The discriminator $D(\cdot; \theta_D) : \mathbb{R}^{l \times d} \rightarrow \mathbb{R}$ is used to approximate the function f that reaches the supremum and its loss is

$$\min_{\theta_D} -\mathbb{E}_{\mathbf{X}} D(\mathbf{X}; \theta_D) + \mathbb{E}_{\mathbf{Z}} D(G(\mathbf{Z}; \theta_G); \theta_D).$$

The generator tries to minimize the Wasserstein-1 distance, which means

$$\min_{\theta_G} \mathbb{E}_{\mathbf{Z}} -D(G(\mathbf{Z}; \theta_G); \theta_D).$$

Note that the discriminator needs to be 1-Lipschitz continuous such that the Kantorovich-Rubinstein duality holds. Thus the authors in [17] proposed to add a gradient penalty to keep the Lipschitz continuity, and the loss for the discriminator becomes

$$\min_{\theta_D} \mathbb{E}_{\mathbf{X}, \mathbf{Z}, \tilde{\mathbf{X}}} -D(\mathbf{X}; \theta_D) + D(G(\mathbf{Z}; \theta_G); \theta_D) + \lambda(\|\nabla_{\tilde{\mathbf{X}}} D(\tilde{\mathbf{X}}; \theta_D)\| - 1)^2$$

where λ is a constant, $\tilde{\mathbf{X}} = (1 - U)\mathbf{X} + U G(\mathbf{Z}; \theta_G)$ is a linear interpolation between \mathbf{X} and $G(\mathbf{Z}; \theta_G)$, and U follows the uniform distribution over $(0, 1)$.